Article

Molecular Cell

β-Hydroxybutyrate Prevents Vascular Senescence through hnRNP A1-Mediated Upregulation of Oct4

Graphical Abstract

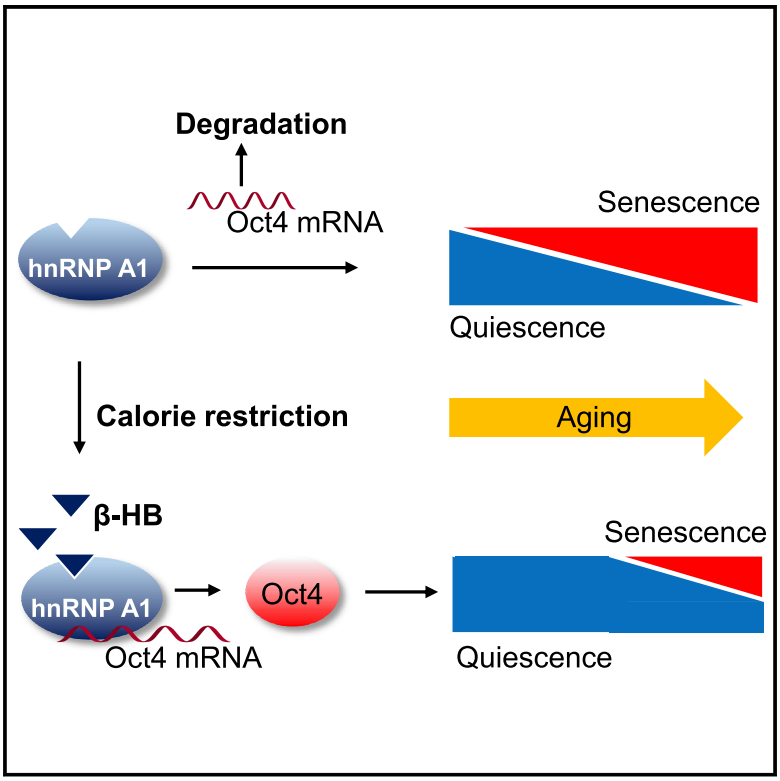

Highlights

- β-hydroxybutyrate prevents the vascular cell senescence
- β-hydroxybutyrate upregulates Oct4 expression via interacting with hnRNP A1
- Oct4-mediated quiescence is able to attenuate hallmarks of senescence
- Circulating β-hydroxybutyrate alleviates the senescence of mouse aorta

Authors

Young-min Han, Tatiana Bedarida, Ye Ding, ..., Qilong Wang, Ping Song, Ming-Hui Zou

Correspondence

psong@gsu.edu (P.S.), mzou@gsu.edu (M.-H.Z.)

In Brief

β-hydroxybutyrate prevents vascular cell senescence via inducing cell quiescence. β-hydroxybutyrate-induced vascular cell quiescence is dependent on Oct4 expression, which is upregulated by forming hnRNP A1 complex with Oct4 mRNA. β-hydroxybutyrate-induced Oct4 expression is negatively correlated with hallmarks of vascular senescence *in vivo*.

Han et al., 2018, Molecular Cell *71*, 1064–1078
September 20, 2018
https://doi.org/10.1016/j.molcel.2018.07.036

CellPress

CellPress

Molecular Cell
Article

β-Hydroxybutyrate Prevents Vascular Senescence through hnRNP A1-Mediated Upregulation of Oct4

Young-min Han,[1] Tatiana Bedarida,[1] Ye Ding,[1] Brian K. Somba,[1] Qiulun Lu,[1] Qilong Wang,[1] Ping Song,[1,*] and Ming-Hui Zou[1,2,*]

[1]Center for Molecular and Translational Medicine, Georgia State University, 157 Decatur Street SE, Atlanta, GA 30303, USA
[2]Lead Contact
*Correspondence: psong@gsu.edu (P.S.), mzou@gsu.edu (M.-H.Z.)
https://doi.org/10.1016/j.molcel.2018.07.036

SUMMARY

β-hydroxybutyrate (β-HB) elevation during fasting or caloric restriction is believed to induce anti-aging effects and alleviate aging-related neurodegeneration. However, whether β-HB alters the senescence pathway in vascular cells remains unknown. Here we report that β-HB promotes vascular cell quiescence, which significantly inhibits both stress-induced premature senescence and replicative senescence through p53-independent mechanisms. Further, we identify heterogeneous nuclear ribonucleoprotein A1 (hnRNP A1) as a direct binding target of β-HB. β-HB binding to hnRNP A1 markedly enhances hnRNP A1 binding with Octamer-binding transcriptional factor (Oct) 4 mRNA, which stabilizes Oct4 mRNA and Oct4 expression. Oct4 increases Lamin B1, a key factor against DNA damage-induced senescence. Finally, fasting and intraperitoneal injection of β-HB upregulate Oct4 and Lamin B1 in both vascular smooth muscle and endothelial cells in mice *in vivo*. We conclude that β-HB exerts anti-aging effects in vascular cells by upregulating an hnRNP A1-induced Oct4-mediated Lamin B1 pathway.

INTRODUCTION

Vascular aging is considered as a main risk factor for developing cardiovascular diseases (CVDs) (Costantino et al., 2016; North and Sinclair, 2012). Cellular aging, known as senescence, mainly contributes to vascular diseases associated with inflammation and dysfunction of the endothelial and smooth muscle cells (Kovacic et al., 2011; Minamino and Komuro, 2007). Despite years of intense study, therapeutic strategies to mitigate vascular diseases through preventing or removing vascular senescence are still required (Childs et al., 2015).

Cellular senescence is an irreversible cell-cycle arrest which restricts the proliferation of abnormal cells. Cellular senescence has multiple physiological functions, including preventing cancer development (Collado and Serrano, 2010) and restricting liver and cardiac fibrosis (Kim et al., 2013). However, the accumulation of senescent cells also contributes to, and can even exacerbate, aging and age-related diseases, such as atherosclerosis (Wang and Bennett, 2012), Alzheimer's disease (Bredesen et al., 2016), and cancer (Finkel et al., 2007). In contrast, cellular quiescence is a reversible cell-cycle arrest and usually occurs due to lack of nutrition or growth factors. Maintaining a quiescent state is thought to be a mechanism by which cells can avoid initiating senescence programs (Salmenperä et al., 2016). Thus, identification of endogenous mechanisms that regulate cell senescence and quiescence may provide novel insights into age-related diseases. It is established that fasting and caloric restriction extend both the average and the maximal lifespan and prevent age-related diseases through energy sensors dependent on Sirtuin 1 (SIRT1) or Forkhead box O3 (FoxO3) activation (Martin et al., 2006). Additionally, calorie restriction-mediated moderation of cell senescence is reported in recent studies (Anton et al., 2013; Ning et al., 2013). However, it is unknown whether alternative metabolic fuels generated during energy deficit, such as the ketone bodies β-hydroxybutyrate (β-HB) and acetoacetate (AcAc), affect cell senescence and quiescence, nor what the underlying mechanisms may be.

Quiescence not only avoids initiation of the senescent program but also contributes to the maintenance of stemness, allowing cells to be resistant to genotoxic stress, a major trigger of cellular senescence (Cai et al., 2004; van Deursen, 2014). Octamer-binding transcriptional factor 4 (Oct4, POU5F1), a regulator of pluripotency in embryonic stem cells, was once thought to be permanently silenced in adult somatic cells (Lengner et al., 2008). Interestingly, a recent study suggests that Oct4 is reactivated in adult vascular smooth cells, as demonstrated by its protective role against atherosclerosis (Cherepanova et al., 2016). However, other functions of Oct4 reactivation remain undefined. In addition, the upstream molecules which regulate Oct4 expression at the posttranscriptional level are also poorly characterized.

Recent studies suggest that Oct4 expression can be regulated by heterogeneous nuclear ribonucleoproteins A2/B (hnRNP A2/B), a subfamily of the large A-U hnRNP family (Choi et al., 2013). hnRNP A1 is a member of the hnRNP family that plays a critical role in RNA processing, including alternative mRNA splicing, transcriptional regulation (Jean-Philippe et al., 2013), and stabilization of mRNA under various stress conditions via formation of stress granules (Guil et al., 2006). However, it remains unknown precisely how these proteins interact.

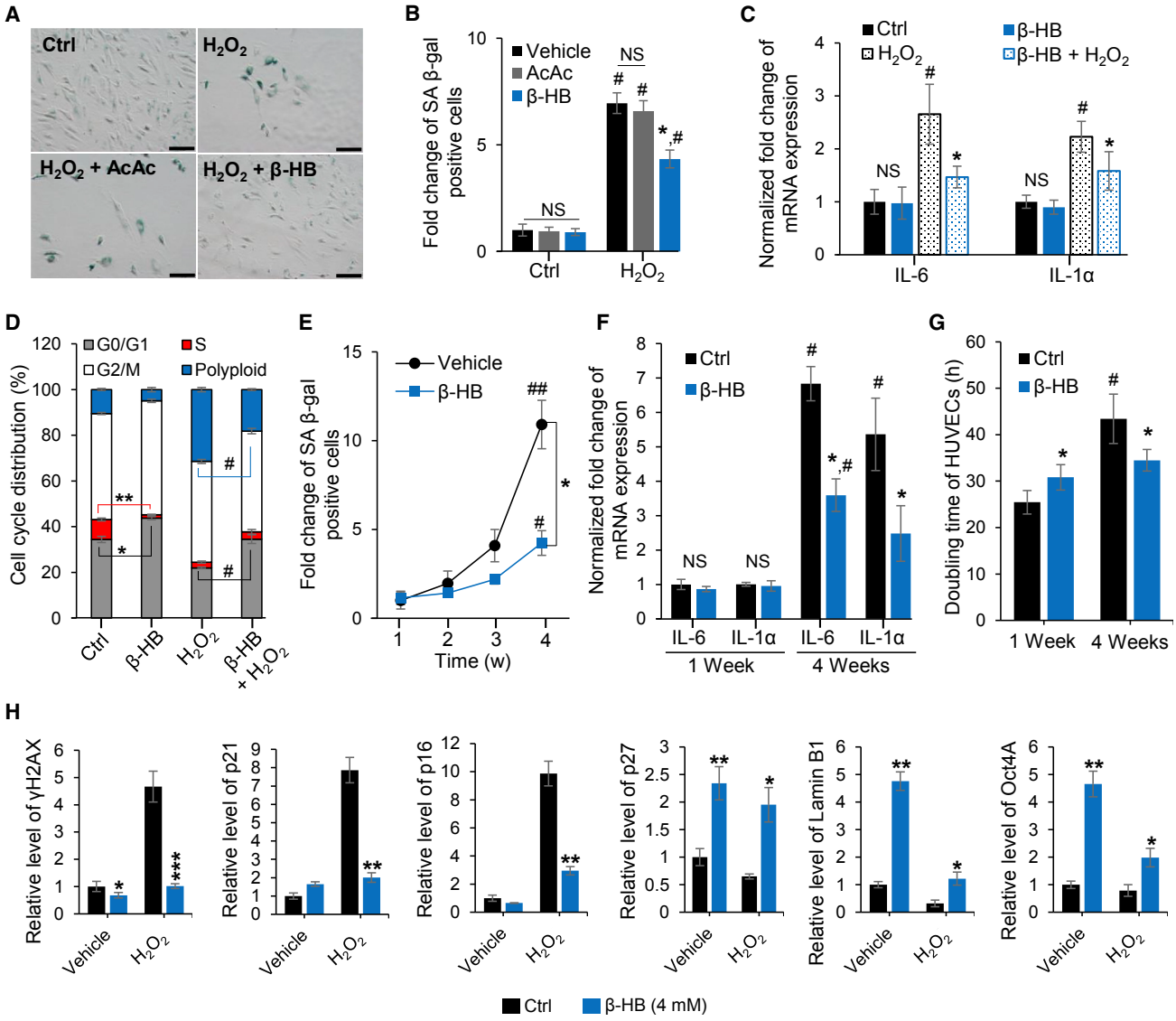

Figure 1. β-Hydroxybutyrate Prevents Cellular Senescence

(A) Representative images of senescence-associated β-galactosidase (SA β-gal) staining. Cultures were exposed to hydrogen peroxide (H_2O_2, 150 μM, 3 days) with or without β-HB (4 mM) or acetoacetate (AcAc, 4 mM) for 3 days. n = 3. Scale bar, 100 μm.

(B) Quantitative analysis of the SA β-gal-positive cells in Figure 1A. n = 3; NS, non-significant; $^{\#}p < 0.05$, control versus H_2O_2; $^{*}p < 0.05$, H_2O_2 versus H_2O_2 + β-HB.

(C) Quantitative real-time PCR (qRT-PCR) of IL-6 and IL-1α mRNA after exposing to β-HB (4 mM) with or without H_2O_2 (150 μM) for 3 days. n = 3, $^{\#}p < 0.05$ control versus H_2O_2, $^{*}p < 0.05$ H_2O_2 versus H_2O_2 + β-HB.

(D) Cell-cycle distribution analysis of HUVECs after β-HB (4 mM) treatment for 3 days with or without H_2O_2 (150 μM). n = 3, $^{*}p < 0.05$, $^{**}p < 0.001$ control versus β-HB, $^{\#}p < 0.05$ H_2O_2 versus H_2O_2 + β-HB.

(E) Time course of the effect of β-HB on SA β-gal activity in HUVECs. n = 3, $^{*}p < 0.05$ vehicle versus β-HB, $^{\#}p < 0.05$, $^{\#\#}p < 0.01$ 1-week treated versus 4-week treated.

(F) qRT-PCR analyses of IL-6 and IL-1α mRNA levels in β-HB (4 mM)-treated HUVECs. n = 3, $^{\#}p < 0.05$, 1-week control versus 4-week control; $^{*}p < 0.05$, 4-week control versus 4-week β-HB.

(G) Effect of β-HB on HUVECs doubling time. n = 3, $^{\#}p < 0.05$, 1-week control versus 4-week control; $^{*}p < 0.05$, 4-week control versus 4-week β-HB.

(H) Alteration of senescence markers (γH2AX, p21, or p16) and quiescence markers (p27, Lamin B1, or Oct4A) in hASMCs treated with or without β-HB for 24 hr. n = 3, $^{*}p < 0.05$, $^{**}p < 0.01$, $^{***}p < 0.001$ control versus β-HB treatment.

Data are presented as mean ± SEM. NS, non-significant; Ctrl, control.

Elevation of ketone bodies, such as β-HB, during fasting or caloric restriction is believed to induce anti-aging effects and alleviate aging-related neurodegeneration (Paoli et al., 2014; Tieu et al., 2003). However, whether ketone body alters pathways in the aging process, specifically the senescence signal in vascular cells, remains unknown. Here we report that

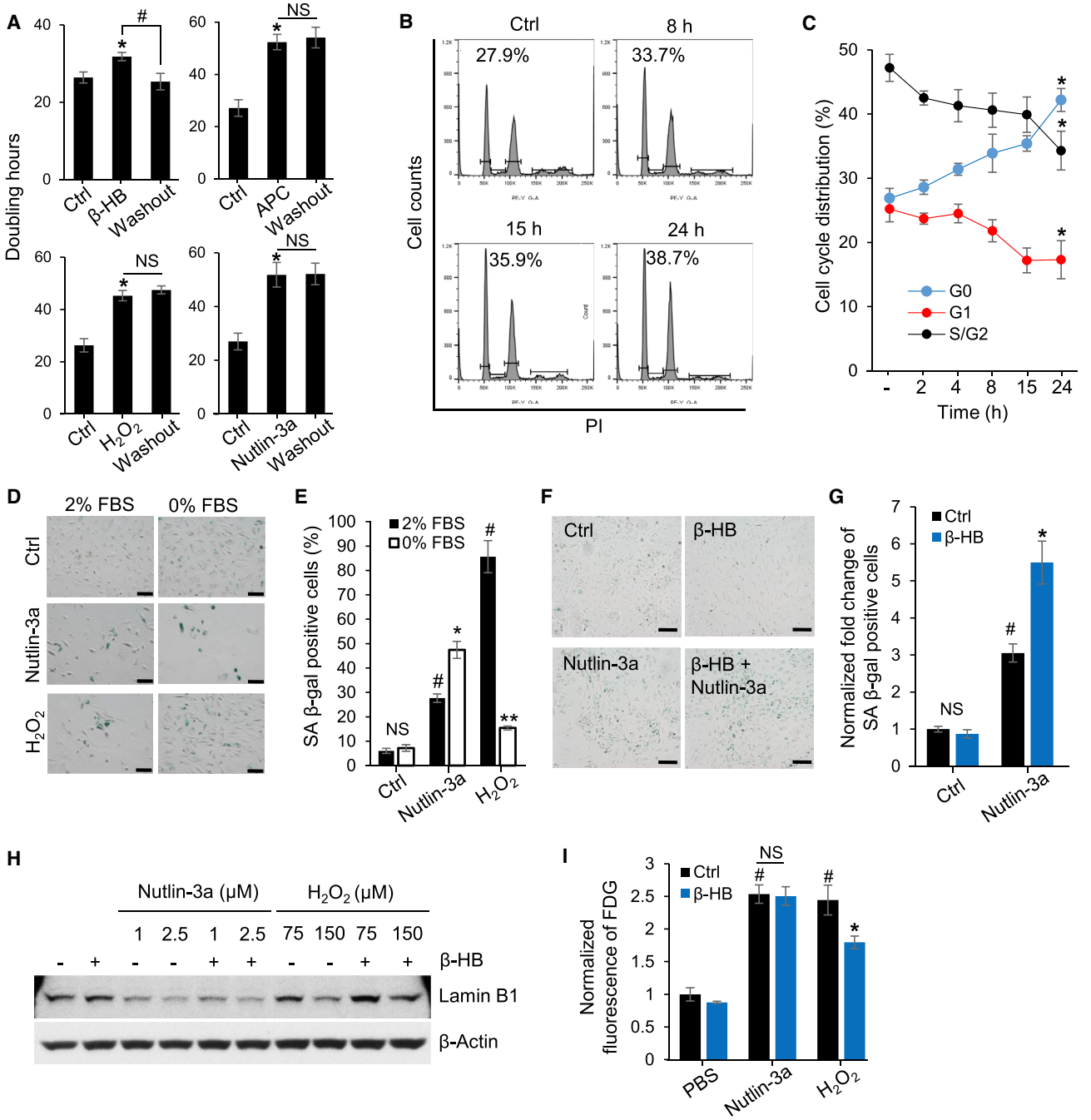

Figure 2. β-HB Induces Human Umbilical Vein Endothelial Cells' Quiescence

(A) Doubling time of HUVECs treated with β-HB (4 mM, 15 hr), H_2O_2 (150 μM, 15 hr), APC (aphidicolin, 2 μM, 15 hr), Nutlin-3a (2.5 μM, 15 hr), and washout groups for each treatment. n = 3, *p < 0.05 control versus treated, #p < 0.05, β-HB versus washout.

(B) Cell-cycle distribution analysis of HUVECs in the G0/G1 phase after β-HB treatment for the indicated time periods.

(C) Cell-cycle distribution of HUVECs in the G0, G1, and S/G2 phases after β-HB treatment for the indicated time periods, assessed with flow cytometry after Pyronin Y and Hoechst 33342 staining. n = 3, *p < 0.05 control versus β-HB-treated (24 hr).

(D) Representative images of SA β-gal activity assays of Nutlin-3a (2.5 μM, 15 hr) or H_2O_2 (150 μM, 15 hr)-induced senescent HUVECs cultured with nutrient-complete media (2% FBS, EGF, bovine brain extract) or FBS-deprived media (0% FBS, EGF, bovine brain extract). n = 3. Scale bar, 100 μm.

(E) Quantitation of Figure 2D. n = 3; NS, non-significant; #p < 0.05, Control (Ctrl) versus Nutlin-3a or H_2O_2 (2% FBS); *p < 0.05, **p < 0.01 H_2O_2 (2% FBS) versus H_2O_2 (0% FBS).

(F) Representative images of SA β-gal staining in Nutlin-3a-treated HUVECs with or without β-HB (4 mM, 15 hr). n = 3. Scale bar, 100 μm.

(G) Quantitation of Figure 2F. n = 3, #p < 0.05, control (Ctrl) versus Nutlin-3a; *p < 0.05, Nutlin-3a versus Nutlin-3a + β-HB.

(legend continued on next page)

β-HB-induced cellular quiescence significantly inhibits both stress-induced premature senescence and replicative senescence through its binding with hnRNP A1, which can bind to and stabilize Oct4 mRNA, thus upregulating Oct4 expression at the posttranscriptional levels.

RESULTS

The Preventative Effect of β-Hydroxybutyrate on Stress-Induced Premature and Replicative Senescence in Vascular Cells

Hydrogen peroxide (H_2O_2) triggers stress-induced premature senescence (SIPS) by increasing oxidative stress (Liu et al., 2014). To test the anti-senescence efficacy of β-HB, primary human umbilical vein endothelial cells (HUVECs) and human aortic smooth muscle cells (hASMCs) (Figure S1A) were exposed to H_2O_2 with or without β-HB. As expected, H_2O_2 (150 μM, 3 days) exposure increased numbers of senescence-associated β-galactosidase- (SA β-gal) positive cells (Figures 1A, 1B, and S1B) with senescence-related morphological transformations: enlarged, flat, and multinucleated appearance of cells (Figure S1C). The addition of β-HB (4 mM, 3 days) markedly reduced senescence, while acetoacetate (AcAc, 4 mM, 3 days) had no effects on H_2O_2-induced senescence (Figure 1B). As expected, β-HB also prevented senescence-related morphological transformations (Figure S1C). These results indicate that the anti-senescence effect by ketone bodies is β-HB specific.

The proinflammatory cytokines IL-6 and IL-1α are proven markers of the senescence-associated secretory phenotype (SASP) (Tchkonia et al., 2013; Zhu et al., 2014). Quantitative real-time PCR (qRT-PCR) of HUVECs samples indicated that β-HB effectively suppressed the expression of IL-6 and IL-1α triggered by H_2O_2 (Figure 1C).

Since multi-nuclei formation is frequently observed in senescence (Sadaie et al., 2015), cell-cycle analysis was used and demonstrated that β-HB treatment led to accumulation at G0/G1 phase and significant reduction of S phase. Moreover, β-HB strongly prevented H_2O_2-induced polyploidy formation (Figures 1D and S1D). These results provided initial evidence for the efficacy of β-HB in preventing SIPS.

In order to test if β-HB prevents replicative senescence (RS), SA β-gal activity was measured weekly for 4 weeks. As shown in Figures 1E and S1E, maintaining HUVECs for 4 weeks markedly induced a replicative senescence, but cell culture for 1 week did not induce a senescence. Therefore, β-HB treatment for 4 weeks decreased the doubling time (Figure 1G) and retained higher proliferative potentials (Figure S1F), which may be due to the decreased senescence. On the other hand, cell culture for 1 week did not induce senescence (Figure 1E), while β-HB treatment for 1 week increased the doubling time (Figure 1G) and modestly decreased the cell number, which may be due to the induction of quiescence by β-HB. Additionally, SASP expression of senescent HUVECs was also reduced by 4-week β-HB treatment (Figure 1F). These results suggest that β-HB induces reversible growth arrest, also known as a cellular quiescence, and thus prevents subsequent senescence.

In order to define the molecular mechanisms by which β-HB exerts anti-senescence effects in vascular cells, we monitored DNA damage repair markers and cell-cycle-regulatory proteins. As shown in Figure S1G, β-HB reduced the levels of γH2AX, a marker of DNA damage (Xu et al., 2015), in both HUVECs and hASMCs. However, β-HB did not affect the phosphorylation of CHK1, BRCA1, or p53 level in either cell line, implying that β-HB-mediated alleviation of senescence is not via enhancement of DNA repair signaling (Williams and Schumacher, 2016; Wu et al., 2010; Yarden et al., 2002). Moreover, β-HB dose-dependently upregulated levels of the cell cycle regulatory proteins p21 (Figure S1G) and p27 (Figure 1H) in normally conditioned cells. Taken together, these results indicate that β-HB-mediated reduction of DNA damage is a consequence of cell-cycle retardation caused by quiescence.

To verify the impact of β-HB on cell-cycle regulation, we compared levels of multiple proteins involved in senescence or quiescence in non-stressed and oxidant-stressed hASMCs treated with β-HB. β-HB markedly suppressed the oxidant-induced elevation of senescence markers (γH2AX, p21, p16). In the non-stress condition, β-HB significantly upregulated quiescence markers (p27, Lamin B1, Oct4A) (Figure 1H). These findings support the hypothesis that β-HB-induced quiescence may help prevent senescence in vascular cells.

β-HB-Induced Cellular Quiescence Is p53 Independent

Next, we investigated the effect of β-HB on cellular quiescence. First, we measured the doubling time of HUVECs to determine if growth arrest by β-HB is reversible. Three senescence inducers, H_2O_2, Aphidicolin (APC), and Nutlin-3a, caused irreversible growth arrest of HUVECs. However, β-HB (4 mM) caused reversible growth arrest, which is the defining feature of quiescent cells (Figure 2A). Cell-cycle retardation at the G0/G1 phage was gradually increased by β-HB treatment in a time-dependent manner (Figure 2B). To prove β-HB-induced cell quiescence, flow cytometry analysis was conducted to measure the reduction of the transcriptome as a marker of cellular quiescence (Cheung and Rando, 2013). As expected, β-HB (4 mM) time-dependently decreased the fluorescence intensity of Pyronin Y, used to quantify total RNA (Will et al., 2013) (Figures 2C, S2A, and S2B). Quantitation of cell-cycle distribution showed that β-HB dramatically induced G0 with simultaneous reductions of G1 and S/G2 phases (Figure 2C). To provide additional evidence of β-HB-mediated quiescence, we tested several molecular markers for quiescence after β-HB treatment, including AMPKα phosphorylation (Thr172) (Saldivia et al.,

(H) Representative western blots for Lamin B1 in HUVECs treated with Nutlin-3a (1 or 2.5 μM, 15 hr) or H_2O_2 (75 or 150 μM, 15 hr) with or without β-HB (4 mM, 15 hr). n = 3.

(I) Effects of β-HB on fluorescein di-β-D-galactopyranoside (FDG) assay. HUVECs were treated with Nutlin-3a (2.5 μM, 15 hr) or H_2O_2 (150 μM, 15 hr) in the presence or absence of β-HB (4 mM, 15 hr). Excitation/emission = 490/514 (nm); n = 3; $^{\#}p < 0.05$, PBS versus Nutlin-3a or H_2O_2; $^{*}p < 0.05$, H_2O_2 versus H_2O_2 + β-HB.

Data are presented as mean ± SEM. NS, non-significant.

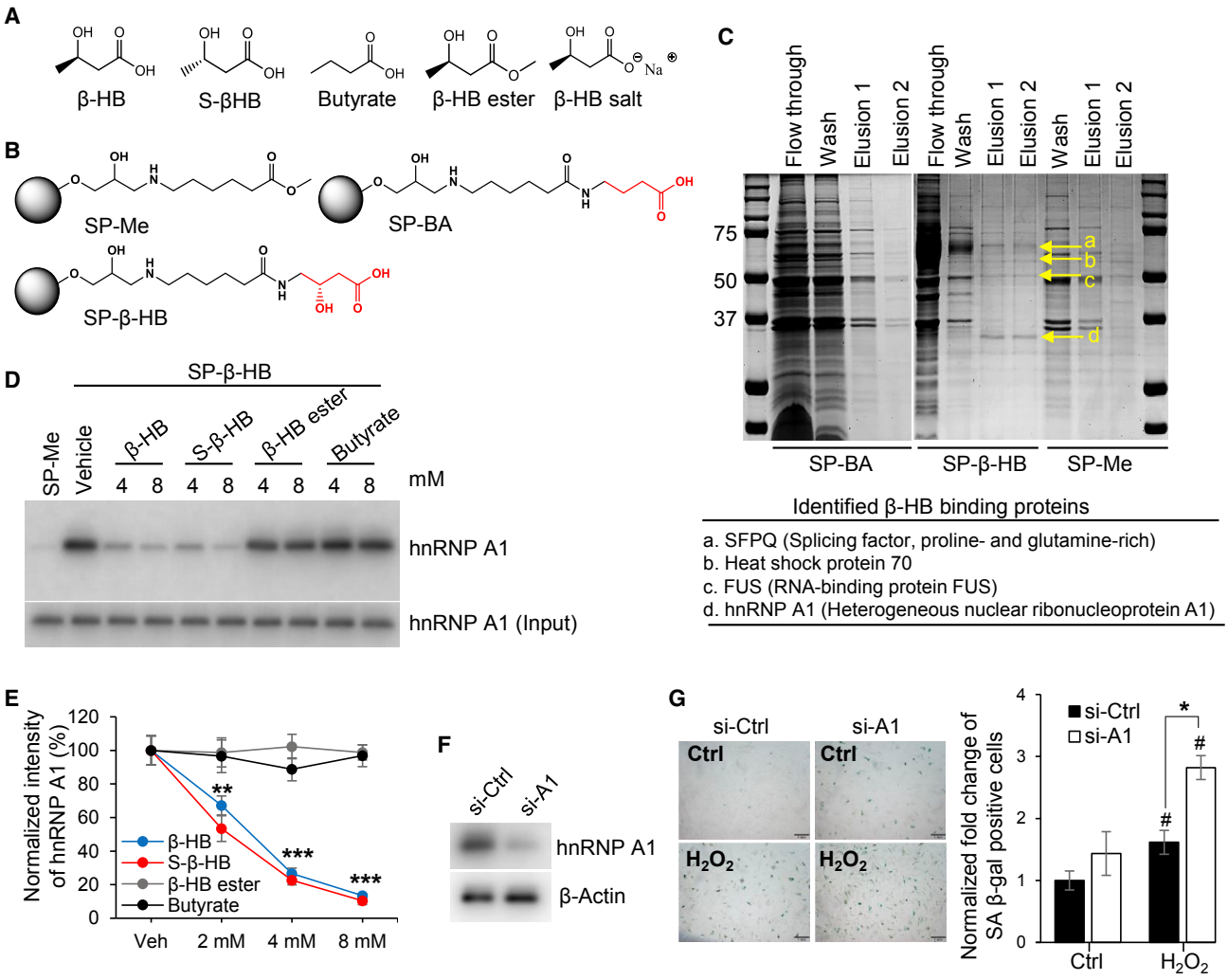

Figure 3. Proteomics Approach to Identify the Target Protein of β-HB Action

(A) Structures of β-HB and its analogs: S-β-HB, Butyrate, β-HB ester, and β-HB salt.

(B) Structures of negative control beads (SP-Me), β-HB, and butyrate-conjugated Sepharose beads (SP-β-HB and SP-BA).

(C) Representative image of affinity chromatography using SP-β-HB, SP-BA, and SP-Me. Binding proteins were eluted with β-HB gradient buffer (0.1 M Tris-HCl, β-HB 0.5–8 mM), then stained with Coomassie brilliant blue dye. Four proteins (SFPQ, heat shock protein 70, FUS, and hnRNP A1) were identified by MALDI TOF MS.

(D) Representative western blots obtained from three individual experiments. Pull-down assays using SP-Me (negative control) and SP-β-HB (positive control). Cell lysates were pretreated with competitors (β-HB, S-β-HB, β-HB ester, and Butyrate) to validate specific binding with hnRNP A1. n = 3.

(E) Quantitation of Figure 3D. $^{**}p < 0.01$, $^{***}p < 0.001$ vehicle versus treated.

(F) Representative western blots for hnRNP A1 showing the knockdown efficiency of siRNA targeting hnRNP A1.

(G) Representative images of SA β-gal staining and quantitation of SA β-gal-positive cells in hnRNP A1-silenced HUVECs treated with or without H_2O_2 (150 μM). Scale bar, 1 mm. $^{\#}p < 0.05$, control versus H_2O_2; $^{*}p < 0.05$, H_2O_2 + si-Ctrl versus H_2O_2 + si-A1.

Data are presented as mean ± SEM. NS, non-significant; si-Ctrl, control siRNA; si-A1, hnRNP A1 siRNA.

2016), S6K dephosphorylation (Thr389), and p27 elevation. We also observed that β-HB significantly and time-dependently induced Lamin B1 expression (Figure S2C), which is known to inhibit the G1/S transition (Shimi et al., 2011). These results support β-HB-mediated cell quiescence. Due to ambiguous roles of quiescence and senescence proteins, several specific molecular markers for quiescence were tested to validate cell status. Figure S2D showed that contact inhibition or fetal bovine serum (FBS) deprivation upregulated p27, p21, Lamin B1, and nucleophosmin 1 (NPM1) in quiescent HUVECs, and these increases were negatively associated with proliferation markers, p-p70 (T389) and p-RB (S807, S811). We compared p27, p21, and Lamin B1 levels between FBS deprivation-induced quiescent and H_2O_2-induced senescent hASMCs in Figure S2E, and SA β-gal activities in quiescence and senescence are shown in Figure S2F. p53 activation and γH2AX upregulation were specifically detected in senescent cells. We found that p27 and Lamin B1, as well as the Oct4, which can activate in vascular smooth

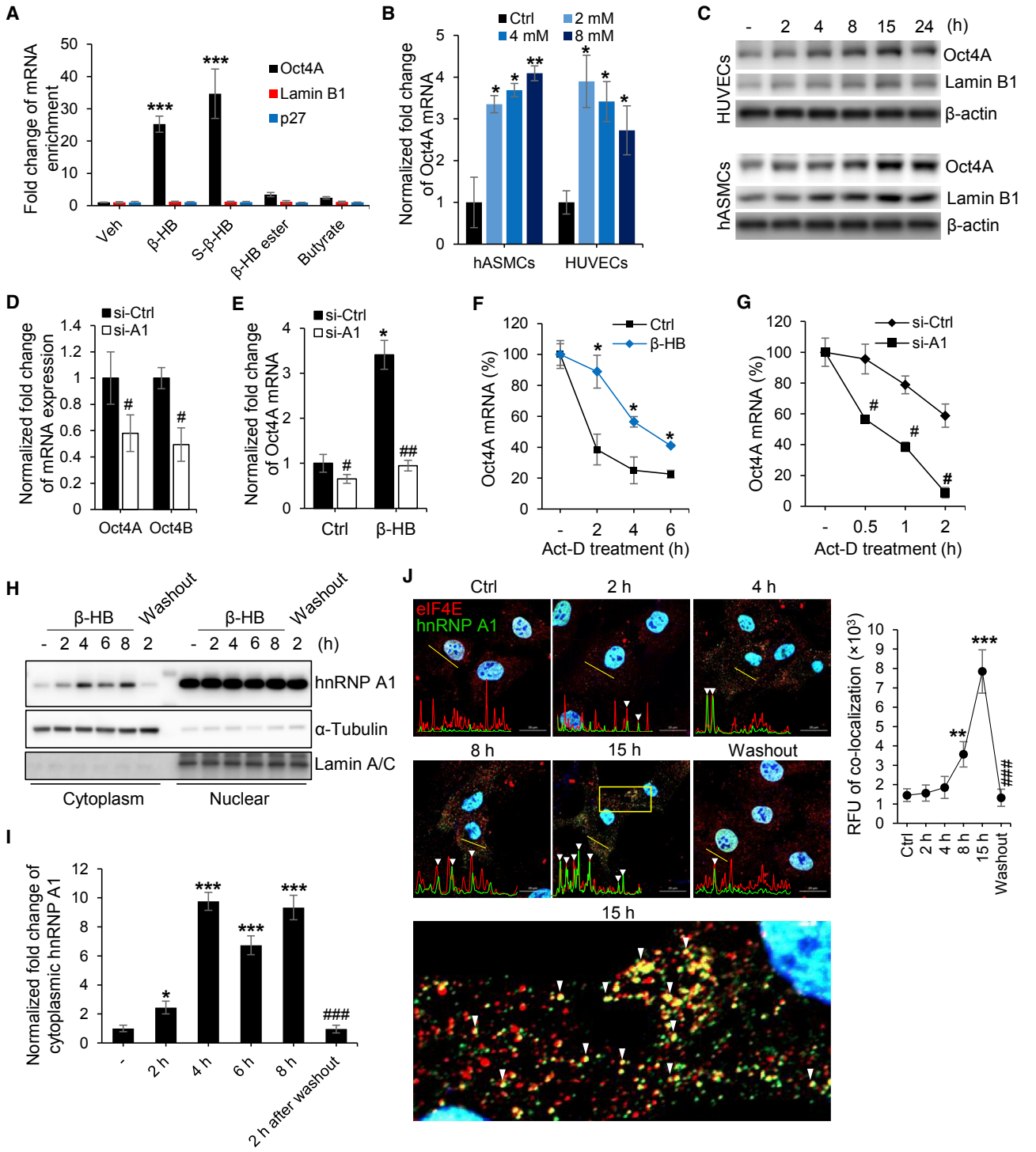

Figure 4. hnRNP A1 Mediates Oct4 mRNA Stabilization in the Presence of β-HB

(A) RNA-immunoprecipitation (RIP) using cytoplasmic hnRNP A1 to assess binding of Oct4, Lamin B1, and p27 mRNAs with hnRNP A1 in the presence of β-HB (4 mM, 15 hr) or β-HB analogs (S-β-HB, β-HB ester, and butyrate, 4 mM, 15 hr). n = 3; ***$p < 0.001$, vehicle versus treated groups.

(B) Quantitative reverse transcription polymerase chain reaction (qRT-PCR) analysis of Oct4A mRNA expression in hASMCs and human umbilical vein endothelial cells (HUVECs) treated with β-HB at the indicated concentrations for 15 hr. n = 3, *$p < 0.05$, **$p < 0.01$ control versus β-HB-treated groups.

(C) Representative western blots for Oct4A and Lamin B1 in HUVECs and hASMCs after β-HB treatment for the indicated time points. n = 3.

(D) qRT-PCR analysis of Oct4A and Oct4B mRNA in HUVECs transfected with si-Ctrl or hnRNP A1 siRNA. n = 3; #$p < 0.05$, si-Ctrl versus si-A1.

(legend continued on next page)

muscle cells (Cherepanova et al., 2016), were up- and downregulated in quiescence and senescence, respectively. Based on these results, p27, Lamin B1, and Oct4 were considered useful markers of quiescence.

To test if β-HB inhibition of senescence is dependent on the p53 pathway, we used the MDM2 (E3 ubiquitin ligase for p53) inhibitor Nutlin-3a to induce p53-dependent senescence. Serum-deprivation-induced quiescent cells were resistant to senescence induced by H_2O_2. However, quiescence did not prevent the senescence trigged by Nutlin-3a (2.5 μM, 15 hr), which induces robust upregulation of p53 and p21, causing p53-dependent senescence (Figures 2D and 2E). Additionally, serum deprivation promoted Nutlin 3a-induced cell death but prevented H_2O_2-induced cell death (Figures S2G and S2H). These results indicate that anti-senescence triggered by quiescence accumulation is p53 independent.

We further evaluated the anti-senescence efficacy of β-HB in case of p53-medicated senescent HUVECs. Interestingly, β-HB accelerated the senescence stimulated by Nutlin-3a treatment (Figures 2F and 2G) and did not affect Nutlin-3a-induced growth arrest (Figure S2I). Taken together, β-HB-mediated alleviation of senescence is p53 independent.

Serum-deprivation- and contact inhibition-induced quiescent cells exhibited p27 and Lamin B1 upregulation. The levels of p27 and Lamin B1 were distinctly upregulated in quiescent cells induced by either serum deprivation or contact inhibition, compared to proliferative cells (Figures S2D and S2E). Additionally, expression of NPM1, which is involved in chromatin organization (Martin et al., 2009), was also associated with Lamin B1 expression (Figure S2D). Lamin B1 was downregulated in senescent HUVECs triggered by Nutlin-3a or H_2O_2 treatment. Hence, H_2O_2-mediated Lamin B1 loss was partially recovered by co-treatment with β-HB, but not in the case of Nutlin-3a-induced senescence (Figure 2H). Additionally, Lamin B1 level was inversely proportional to cell senescence (Figures 2H and 2I). Taken together, these results suggest that β-HB induces cell quiescence via Lamin B1 upregulation, which prevents oxidative stress-induced senescence in a p53-independent manner.

hnRNP A1 Is a Direct Target of β-HB in Regulating Cell Quiescence

There are several derivatives of β-HB, including S-β-HB, β-HB ester, β-HB salt, and butyrate (Figure 3A). Interestingly, only S-β-HB, which is an enantiomer of β-HB, and β-HB salt, which is a pH-neutralized form of β-HB, both inhibited the H_2O_2-induced SASP (IL-6 and IL-1α) transcriptional expression in a similar manner to β-HB treatment (Figure S3A). These results suggest that both the β hydroxyl and carboxylic acid groups are required for the activity of β-HB. However, lower pH caused by β-HB treatment, as well as changes in the R-S configuration to a γ carbon of β-HB, did not affect the activity of β-HB. Therefore, the γ carbon of β-HB was modified to elongate the linker for affinity chromatography.

Two negative control beads, SP-Me and SP-BA, were compared with β-HB-conjugated beads (SP-β-HB) (Figure 3B). To identify β-HB-binding protein(s), affinity chromatography was performed using β-HB-conjugated Sepharose beads compared to a negative control (Figure 3C). We identified hnRNP A1 as a β-HB-binding protein using MALDI-TOF mass analysis. To confirm binding affinity, a pull-down assay was performed using SP-β-HB beads, and hnRNP A1 was validated with a specific antibody. The binding between hnRNP A1 and β-HB-conjugated beads was disturbed when the interaction was challenged with excess β-HB, S-β-HB, β-HB ester, or butyrate acting as binding competitors (Figures 3D and 3E). Furthermore, silencing hnRNP A1 triggered senescence of HUVECs and accelerated the response to H_2O_2 (Figures 3F and 3G).

As depicted in Figure 3C, β-HB also weakly bound two additional proteins, identified by mass spectrometry as Splicing factor proline- and glutamine-rich (SFPQ) and RNA-binding protein FUS (FUS). However, silencing SFPQ or FUS did not significantly induce senescence (Figures S3B and S3C). 2-D proteomics analysis (Figure S3D) showed that β-HB treatment barely altered proteomes with the exception of NPM1. Because NPM1 regulates quiescence (Ito et al., 2010) and cooperatively acts with Lamin B1 (Martin et al., 2009), NPM1 upregulation might be involved in quiescence associated with β-HB-mediated Lamin B1 upregulation.

Oct4A Upregulation by hnRNP A1

To determine the association between hnRNP A1 and Oct4 mRNAs, RNA-immunoprecipitation assays were performed in the presence or absence of β-HB. The binding of hnRNP A1 with Oct4 mRNA was enriched by treatment of β-HB or S-β-HB. In addition, β-HB ester and butyrate, which has no effect on SASP inhibition, did not affect the interactions between hnRNP A1 and Oct4A mRNA (Figure 4A).

Although β-HB has biphasic induction of Oct4 mRNA in HUVECs, β-HB (2–4 mM) markedly increased Oct4 mRNA levels in both HUVECs and hASMCs (Figure 4B). A dual luciferase assay indicated that transcriptional activity of Oct4A was enhanced by β-HB and S-β-HB, whereas butyrate and niacin

(E) qRT-PCR analysis of Oct4A mRNA in control siRNA-transfected or hnRNP A1-silenced HUVECs treated with or without β-HB (4 mM, 15 hr). n = 3, $^{\#}p < 0.05$, $^{\#\#}p < 0.01$ si-Ctrl versus si-A1, $^{*}p < 0.05$ control versus β-HB-treated group.
(F) Regulation of Oct4 mRNA stability by β-HB treatment (4 mM, 15 hr) in HUVECs treated with actinomycin D. By blocking transcription with actinomycin D (6.5 μg/ml), the half-life of Oct4A mRNA was demonstrated at various times after adding actinomycin D. n = 3, $^{*}p < 0.05$ control versus β-HB.
(G) Oct4 mRNA stability analysis in hnRNP A1-silenced HUVECs by actinomycin D application in a time-dependent manner. n = 3; $^{\#}p < 0.05$, si-Ctrl versus si-A1.
(H) Representative western blots for subcellular hnRNP A1 localization after β-HB treatment (4 mM, 2–8 hr). α-tubulin and Lamin A/C were used to normalize results for the cytoplasm and nucleus, respectively.
(I) Quantification of Figure 4H. n = 3, $^{*}p < 0.05$, $^{***}p < 0.001$ control versus β-HB treatment. $^{\#\#\#}p < 0.01$, β-HB-treated (8 hr) versus washout.
(J) Representative immunofluorescence labeling for hnRNP A1 (green) and eIF4E (red) in hASMCs after β-HB treatment and washout. Linear trajectories crossing the cell with the two signals were shown by yellow line. White triangles indicate colocalization of eIF4E and hnRNP A1. Quantification of colocalization is presented at the right side of image. n = 3; scale bar, 20 μm. $^{**}p < 0.01$, $^{***}p < 0.01$, control versus β-HB treatment. $^{\#\#\#}p < 0.001$, 15 hr versus washout.
Data are presented as mean ± SEM.

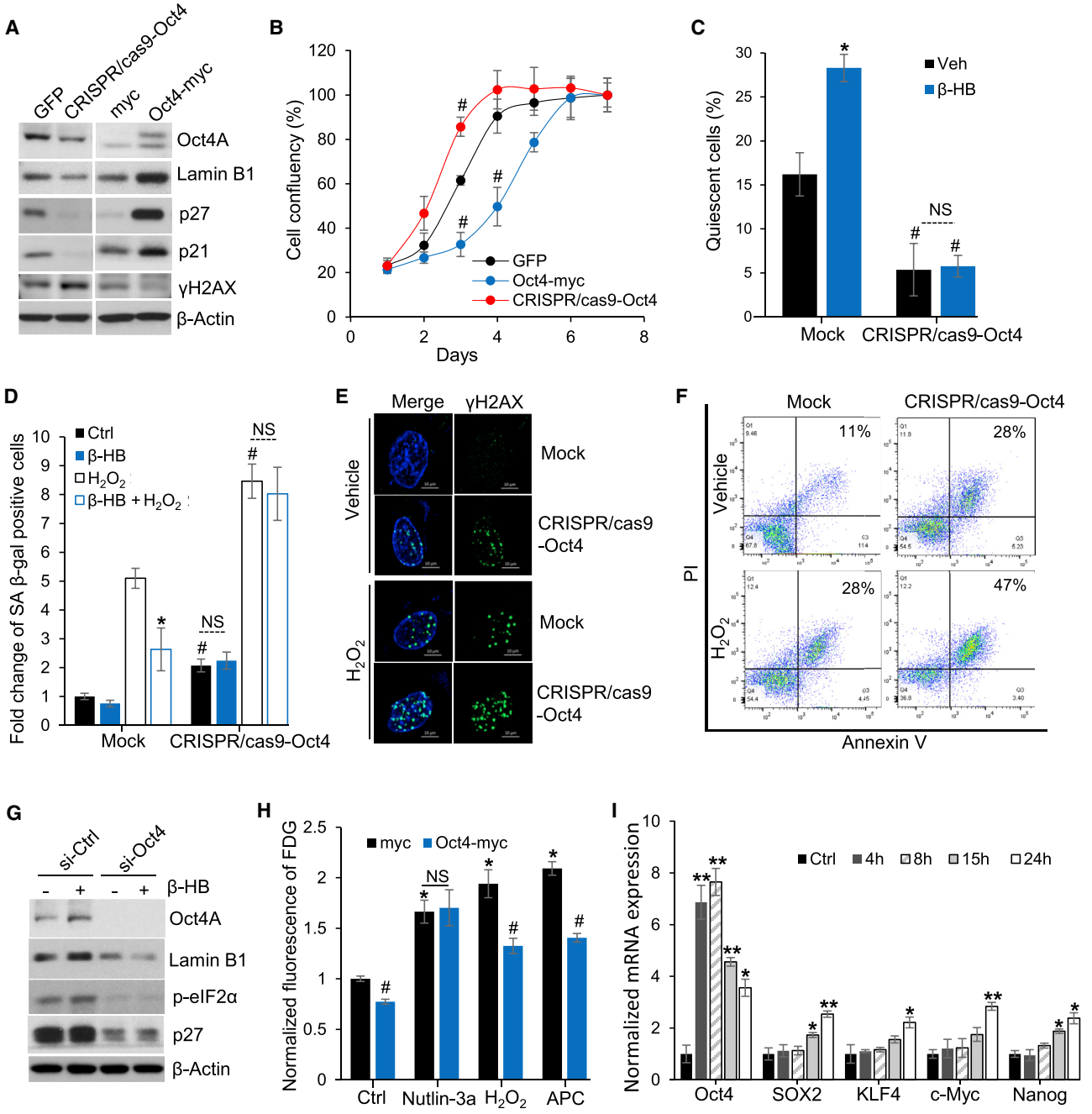

Figure 5. Oct4 Knockdown and Ectopic Expression in Human Umbilical Vein Endothelial Cells

(A) Representative western blots for quiescence- and senescence-associated proteins (Lamin B1, p27, p21, and γH2AX) after Oct4 gene knockdown or overexpression. n = 5.

(B) HUVECs growth rates after Oct4 knockdown or ectopic expression. Following transfection with GFP, Oct4-myc, or CRISPR/cas9-Oct4 plasmid, equal numbers of HUVECs were seeded on plates, and cells were counted daily. n = 3, $^{\#}p < 0.05$, 1 day versus days after seeding.

(C) Cell-cycle distribution of quiescent (G0 phase) HUVECs transfected with/without CRISPR/cas9-Oct4. n = 3, $^{\#}p < 0.05$, mock versus CRISPR/cas9-Oct4; $^{*}p < 0.05$, vehicle versus β-HB. NS, non-significant.

(D) SA β-gal assays of mock or Oct4-knockdown HUVECs after H_2O_2 (150 μM, 24 hr) stimulation with or without β-HB treatment (4 mM, 24 hr). n = 3, $^{*}p < 0.05$ H_2O_2 (Stone et al., 2009) versus β-HB + H_2O_2 (Stone et al., 2009), $^{\#}p < 0.05$ mock versus CRISPR/cas9-Oct4.

(E) Representative immunofluorescent labeling for γH2AX (green) in mock or Oct4 knockdown HUVECs (CRISPR/cas9-Oct4). n = 3. Scale bar, 10 μm.

(F) Apoptosis analysis of mock or Oct4-knockdown HUVECs (CRISPR/cas9-Oct4) stimulated by H_2O_2 (200 μM) for 3 days. n = 3.

(G) Representative western blots for the quiescence markers Lamin B1, p-eIF2α, and p27 in si-Ctrl- or Oct4 siRNA-transfected HUVECs with or without β-HB (4 mM, 15 h) treatment. n = 4.

(legend continued on next page)

did not induce significant changes (Figure S4A). Additionally, Oct4A and Lamin B1 levels in β-HB-treated HUVECs or hASMCs peaked at 15 hr (Figure 4C).

Then the alternative splicing regulation of Oct4 gene by hnRNP A1 was assessed. As shown in Figure S4B, β-HB (4 mM) did not regulate alternative splicing of the Oct4 gene by showing upregulation of both Oct4A and Oct4B. Likewise, both Oct4A and Oct4B mRNA were reduced by hnRNP A1 silencing in HUVECs (Figure 4D). Moreover, the total absence of β-HB-enhanced Oct4 upregulation in hnRNP A1-silenced cells suggests that hnRNP A1 is critical for β-HB-induced Oct4 activation (Figure 4E).

Next, we conducted mRNA stability analysis. The half-life of Oct4 mRNA was effectively extended from 90 min to 5 hr by β-HB treatment (Figure 4F) in transcriptional inhibitor actinomycin D-pretreated HUVECs. Moreover, silencing of hnRNP A1 shorten the half-life of Oct4 mRNA even under normal condition (Figure 4G). These data indicate that Oct4 mRNA is stabilized by hnRNP A1 in the presence of β-HB.

We next determined if Oct4 mRNA stabilization is associated with stress granule formation. Subcellular fractionation results showed that β-HB induced translocation of hnRNP A1 from the nucleus to the cytoplasm (Figures 4H, 4I, and S4C). Furthermore, immunofluorescent staining of hnRNP A1 with stress granule markers, eIF4E and TIA-1, also supported β-HB-mediated transport of hnRNP A1 from the nucleus to the cytoplasm to form stress granules (Figures 4J, S4D, and S4E). Plot of line scan showed a significant correlation between the spatial localization of eIF4E and hnRNP A1 (Figure 4J), or TIA-1 and hnRNP A1 (Figure S4E) in a time-dependent manner of β-HB treatment. These results define the molecular mechanism of β-HB/hnRNP A1-mediated elevation of Oct4.

Functional Role of Oct4A in Cellular Senescence

To validate the new functional role of Oct4 in cellular senescence, we employed the CRISPR/Cas9 knocking down system and a pCMV ectopic expression system. Oct4 positively regulated the expression of p21, p27, and Lamin B1 while negatively regulating the levels of γH2AX. The negative correlation of γH2AX with Oct4 expression indicates that loss of Oct4 triggers cellular senescence by inducing DNA damage. On the contrary, ectopic expression of Oct4 prevents senescence by reducing DNA damage (Figure 5A).

Consistent with the observation that Oct4 increased p27 and Lamin B1 levels (Figure 5A), ectopic Oct4 overexpression retarded cell growth (Figure 5B). Conversely, selective Oct4 knockdown promoted cell growth (Figure 5B). These data imply that Oct4-mediated cell-cycle regulation is strongly related with p27 and Lamin B1-controlled cell quiescence. Oct4 knockdown disrupted β-HB-induced cell-cycle arrest in G0/G1 (Figure S5A), suggesting that Oct4 induces cellular quiescence. Additionally, silencing Oct4 expression could activate p-p70 S6K and p-RB, which are exhibited as proteins synthesis and G1/S transition signaling (Figure S5B). Staining of Pyronin Y and Hoechst33342 further demonstrated that Oct4 knockdown promoted G1/S transition by reducing the quiescent state (Figures 5C and S5C) while inducing senescence (Figure S5D). These data suggest that β-HB-induced quiescence is Oct4 dependent.

To further study the Oct4-dependent preventative effect of β-HB, cell senescence was assessed using Oct4-knockdown HUVECs. SA β-gal assays further demonstrated that the anti-senescence effect of β-HB is mediated by Oct4A (Figures 5D and S5E). Likewise, loss of Oct4A significantly increased SASP expression and countered the preventative effect of β-HB (Figure S5F). To further validate that reduction of quiescence or induction of rapid cell growth is through Oct4 loss and therefore is vulnerable to genotoxic stress, DNA damage and apoptosis were tested using Oct4-silenced HUVECs. As expected, Oct4A knockdown significantly enhanced H_2O_2-mediated DNA damages (Figure 5E) and promoted apoptosis of HUVECs (Figures 5F and S5G).

As depicted in Figure 5G, Oct4A knockdown in HUVECs markedly alleviated β-HB–induced upregulation of the quiescence regulatory proteins Lamin B1, p27, and p-eIF2α. Consistently, Oct4A silencing abolished Lamin B1 transcription (Figure S5H), suggesting that Oct4A is a crucial transcriptional factor for this protein. Conversely, ectopic Oct4A overexpression reduced H_2O_2- and APC-induced senescence. Importantly, Oct4A overexpression did not alter Nutlin-3a-induced senescence, implying that Oct4-mediated senescence alleviation does not require p53 (Figure 5H).

We next assessed whether β-HB treatment alters other Yamanaka factors including SOX2, KLF4, and c-Myc (Takahashi and Yamanaka, 2006). Significant elevation of Oct4A mRNA was observed 4 hr after β-HB treatment (Figure 5I). In contrast, the mRNA levels of SOX2, KLF4, c-Myc, and Nanog were not elevated. Our findings strongly indicate that β-HB-alleviated senescence is Oct4A dependent and does not involve other Yamanaka factors.

Oct4A Upregulation in Vascular Tissue by Acute Elevation of β-HB

To further determine β-HB's effect on Oct4 upregulation *in vivo*, C57BL/6J mice were intraperitoneally injected with β-HB salt or S-β-HB salt (1.5 g/kg body weight) (Figure 6A). As shown in Figure 6B, both β-HB and S-β-HB were able to upregulate Oct4A, Lamin B1, p27, and phospho-eIF2α in thoracic aorta, indicating cell quiescence. Interestingly, β-HB-induced Oct4 protein elevation was only observed in the aorta, brain, and heart (Figure S6A). Oct4A mRNA was also increased by β-HB and S-β-HB injection, especially in the aorta, brain cortex, and heart (Figure 6C). Additionally, S-β-HB, which was not utilized in the ketolysis pathway (Figures S6B and S6C), triggered more significant Oct4A induction than β-HB did (Figure 6C), indicating that Oct4 upregulation

(H) Senescence-associated FDG assay. HUVECs were transfected with myc or Oct4-myc plasmids and treated with Nutlin-3a (2.5 μM, 15 hr), H_2O_2 (150 μM, 15 hr), or APC (2 μM, 15 hr) 2 days after transfection. n = 3, $^{\#}p < 0.05$ myc versus Oct4-myc, $^{*}p < 0.05$ control versus treated. NS, non-significant.

(I) qRT-PCR analyses for Oct4, SOX2, KLF4, c-Myc, and Nanog in HUVECs after β-HB (4 mM) treatment for the indicated times. n = 3, $^{**}p < 0.01$, $^{*}p < 0.05$ control versus treated.

Data are presented as mean ± SEM.

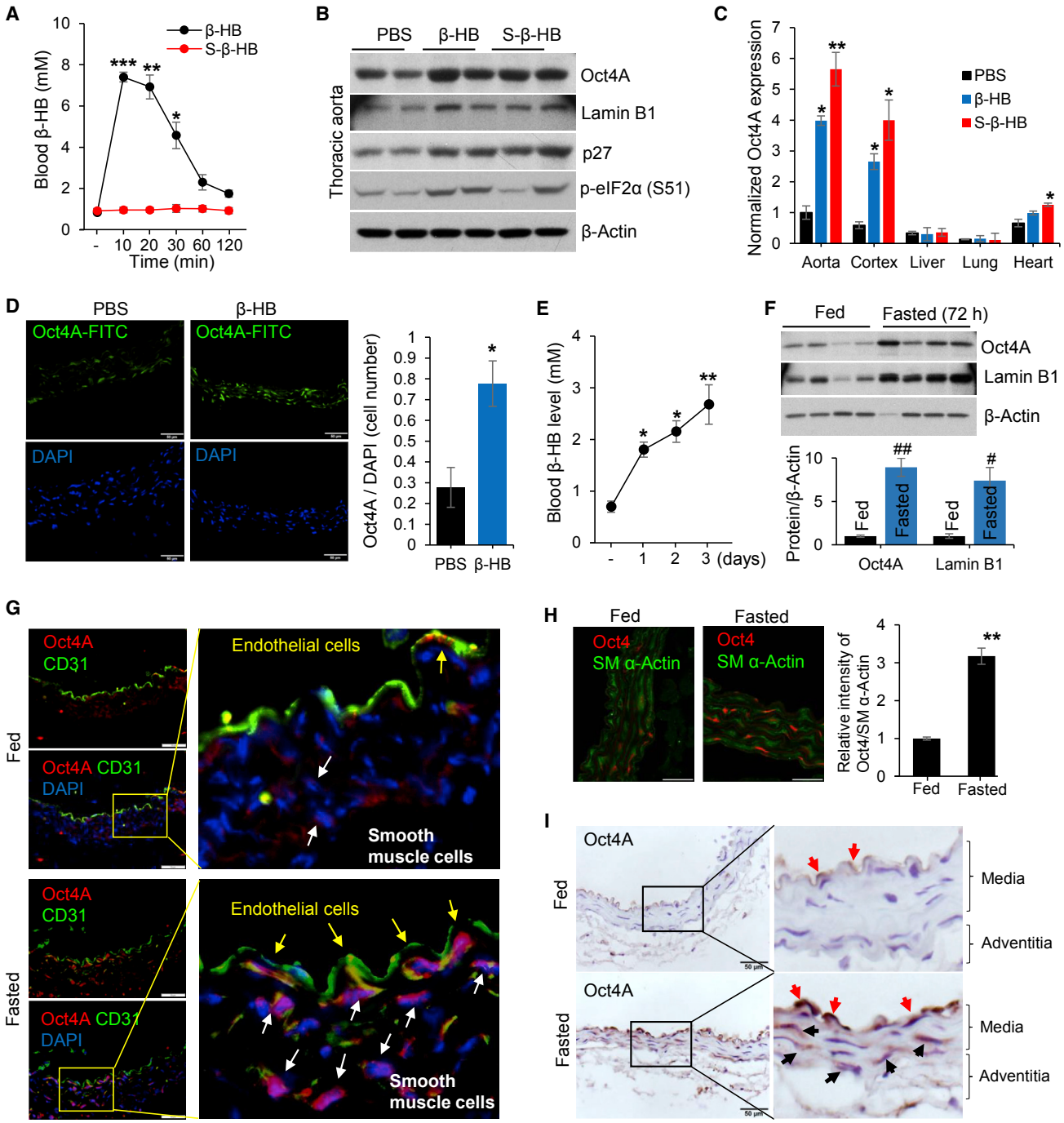

Figure 6. Oct4A Upregulation in Vascular Tissues by β-HB Injection or Fasting

(A) Blood β-HB levels in C57BL/6J mice after intraperitoneal (i.p.) injection of β-HB (1.5 g/kg body weight) or S-β-HB (1.5 g/kg). n = 6/group, *p < 0.05, **p < 0.01, ***p < 0.001, vehicle versus β-HB injection.

(B) Western blotting analysis for Oct4A and other quiescence markers (Lamin B1, p27, and p-eIF2α) in C57BL/6J mice aorta after i.p. injection with PBS, β-HB salt (1.5 g/kg body weight), or S-β-HB salt (1.5 g/kg body weight) dissolved in PBS. n = 6 mice/group.

(C) qRT-PCR analysis of Oct4A expression in various organs after i.p. injection with PBS, β-HB salt, or S-β-HB salt (1.5 g/kg body weight). n = 6 mice/group, *p < 0.05, **p < 0.01, PBS versus β-HB or S-β-HB.

(D) Representative immunofluorescent labeling with a FITC-conjugated Oct4A antibody in C57BL/6J mouse thoracic aorta 4 hr after β-HB injection (1.5 g/kg). Quantitation of Oct4A-positive cells, normalized by DAPI, are shown at right. n = 6 mice/group, *p < 0.05, PBS versus β-HB.

(E) Blood β-HB levels in C57BL/6J mice during fasting for the indicated time periods. n = 6 mice, *p < 0.05, **p < 0.01, feeding versus fasting.

(F) Western blotting analyses of Oct4A and Lamin B1 in thoracic aorta from fed or fasted mice. n = 8 mice/group.

(legend continued on next page)

is independent of energy homeostasis. Moreover, β-HB injection enhanced Oct4A expression as well as the number of Oct4-positive cells in aorta (Figure 6D).

Blood levels of β-HB in C57BL/6J mice were upregulated from 0.7 mM to 2.6 mM by fasting in a time-dependent manner (Figure 6E). Oct4A and Lamin B1 protein levels in thoracic aorta tissue were dramatically elevated by fasting for 72 hr (Figures 6F and S6D). Immunofluorescent staining using anti-CD31, anti-smooth muscle (SM) α-Actin, or anti-Oct4 antibodies demonstrated that 3-day fasting elevated Oct4 expression in endothelial and vascular smooth muscle cells (Figures 6G and 6H). Immunohistochemistry assay also provided evidences for Oct4 upregulation in endothelial and smooth muscle cells during fasting (Figure 6I). These results indicate that acute induction of circulating β-HB upregulates Oct4 and Lamin B1 expression *in vivo*.

Chronic Effect of β-HB on Preventing Senescence in Intermediate Aged Mice

Experiments were performed to determine if maintaining appropriate β-HB blood levels alleviates vascular aging. As shown in Figure S7A, IL-1α, an upstream regulator of IL-6, was elevated in middle-aged mice, whereas IL-6, a major SASP marker, was elevated in aged mice (96 weeks old) (Figure S7B). The concentration of serum β-HB varied in the middle-aged and aged mice from 0.3 to 1.2 mM with a negative correlation with body weight (Figure S7C).

We evaluated if blood β-HB is linked to SASP expression in aged mice (n = 38) with a wide range of blood β-HB (0.3–1.2 mM). As depicted in Figure S7D, low IL-1α levels were found in mice with β-HB concentrations between 0.8 and 1.2 mM, whereas high levels were observed in mice with β-HB concentrations between 0.3 and 0.5 mM. Similarly, the level of IL-6 was negatively associated with β-HB. The expression of both Oct4A and Lamin B1 was positively associated with higher blood β-HB (Figure S7E). Furthermore, staining of whole mouse aorta supported the conjecture that SA β-gal positivity was negatively associated with blood β-HB level (Figures 7A and 7B).

To further assess whether β-HB distinctly affects different parts of the aorta, whole mouse aortas were separated into the aortic arch (Arch) and thoracic aorta (TA), and multiple sections of Arch and TA were examined with SPiDer β-gal assay. As shown in Figures 7C and S7F, the mice with a high level of blood β-HB (1.1 mM) exhibited significant reduction of SA β-gal activity in the Arch and moderate reduction in the TA, compared to those with a low level of β-HB (0.4 mM).

The middle-aged mice (64 weeks old) that maintained a high level of β-HB (1.1 mM) displayed significantly increased expression of Oct4 and Lamin B1 over mice maintained with a 0.6 mM concentration of β-HB. Additionally, the majority of Oct4A expression was mainly co-localized with Lamin B1 (Figure 7D). Plot of line scan demonstrated an increase of expression and a colocalization of Lamin B1 with Oct4A in TA, influenced by a high level of β-HB (1.1 mM). Consistently, aged mice (80 weeks old) with high circulating β-HB (1.0–1.1 mM) had higher Oct4A and Lamin B1 levels than mice with 0.3–0.4 mM circulating β-HB. In addition, thoracic aortas from older animals displayed higher Oct4A expression than aortic arches with senescent phenotypes (Figure 7E).

To further validate a negative relationship of senescence and Oct4A, and to confirm a β-HB-mediated Oct4A elevation, flow cytometry analysis was performed using isolated mouse primary smooth muscle cells (Figure 7F). Here, we demonstrated that high-level β-HB (1.1 mM) upregulated Oct4 expression in primary smooth muscle cells compared to cells with 0.4 mM β-HB (Figure S7G). Oct4-upregulated cells (Oct4 +) exhibited significant reduction of SA β-gal activity compared to Oct4A-downregulated cells (Oct4−) (Figure 7G).

Since advanced atherosclerotic lesions exhibit senescent cells (Childs et al., 2016), we conducted co-staining of SPiDer β-gal and Oct4 in mice aortic roots, which develop atherosclerosis. Most of the senescence-positive areas in lesion were not colocalized with Oct4-expressing cells (Figure 7H). All the data suggest that chronic upregulation of β-HB consequently reduces or delays cellular senescence via upregulating Oct4A expression.

DISCUSSION

In this study, we have demonstrated that β-HB prevents both replicative- and stress-induced senescence in vascular cells and reduces serum levels of the pro-senescence marker IL-1α *in vivo*. This prevention of senescence by β-HB is Oct4A dependent and p53 independent. β-HB mediates Oct4A elevation by direct binding with hnRNP A1 and induces vascular cell quiescence, thus preventing cellular senescence.

Our research provides a novel insight into the mechanism of β-HB-mediated anti-senescence in vascular tissues. Although many studies have focused on the beneficial effects of caloric restriction, which can extend lifespan and delay aging in various species (Colman et al., 2014; Minor et al., 2010), the effect and mechanism of caloric restriction on vascular cell quiescence and senescence remain poorly defined (Minamino and Komuro, 2007; Tian and Li, 2014; Uryga and Bennett, 2016). The principal finding of our study is the identification of the molecular target of β-HB using a ligand fishing approach. Ligand fishing approaches can still be highly effective in identifying the target molecules of small molecules such as pharmaceutic drugs or bio-active metabolites (Spring, 2005). With this approach, we identified that hnRNP A1 is a direct binding target of β-HB and regulates the affinity for its target mRNAs.

(G) Representative immunofluorescent labeling for Oct4A and CD31 in fed or fasted (72 hr) mice aortas. Oct4A-expressing endothelial cells and smooth muscle cells are indicated with yellow and white arrows, respectively. Nuclei were stained with DAPI. Scale bar, 100 μm. n = 4 mice/group.

(H) Representative immunofluorescent labeling for Oct4A and SM α-Actin in fed or fasted (72 hr) mice aortas. Scale bar, 100 μm. n = 4 mice/group. **p < 0.01, feeding versus fasting.

(I) Representative immunohistochemical staining for Oct4A in fed or fasted (72 hr) mice aorta. Red arrow indicates endothelial cells, and black arrow indicates smooth muscle cells. Scale bar, 50 μm. n = 5 mice/group.

Data are presented as mean ± SEM.

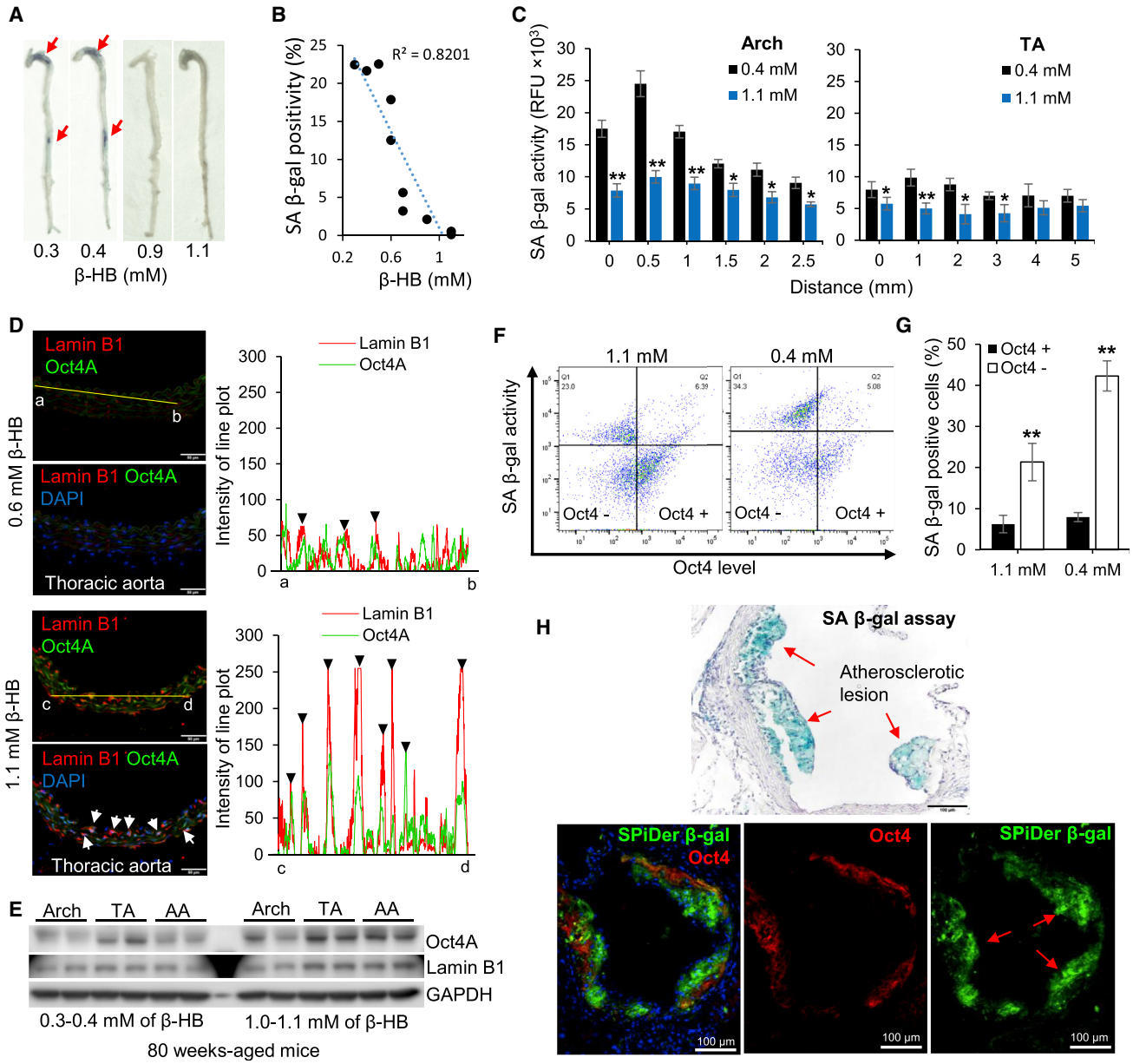

Figure 7. Circulating β-HB Chronically Affects Oct4 Signaling in Aged Mice

(A) SA β-gal activity assays of whole aorta from aged mice (80 weeks old, n = 10) stratified by blood β-HB level.

(B) Quantification of SA β-gal positivity in Figure 7A. SA β-gal activity in mice aorta negatively correlated with blood β-HB level (R^2 = 0.8201).

(C) Fluorogenic β-gal activity assays of multiple sections of aged mice aorta (Arch and Thoracic). Mice were grouped according to blood β-HB level (0.4 and 1.1 mM, n = 6 mice/group), then aorta tissues were reacted with SPiDer β-gal. *p < 0.05, **p < 0.01, 0.4 mM versus 1.1 mM.

(D) Representative immunofluorescence staining for Lamin B1 and Oct4A in 64-week-old mice stratified by blood β-HB concentration (0.6 and 1.1 mM, n = 4 mice/group). Linear trajectories (yellow line) crossing the cell with two signals were presented right side of image. White arrows and black triangles indicate colocalization of Lamin B1 and Oct4A.

(E) Western blotting analyses of Oct4A and Lamin B1 in aged mice (80 weeks old) stratified by blood β-HB concentration (0.3–0.4 mM and 1.0–1.1 mM, n = 6 mice/group).

(F) Flow cytometry analysis of mice primary smooth muscle cells. Aortic smooth muscle cells were isolated from mice stratified by blood β-HB concentration (1.1 mM and 0.4 mM). Isolated aortic smooth muscle cells were reacted with SPiDer β-gal assay, then fixed and stained with Oct4 antibody. n = 6 mice/group.

(G) Quantitative analysis of Figure 7H. SA β-gal positivity according to the level of Oct4. n = 6 mice/group. **p < 0.01 Oct4+ versus Oct4−.

(H) SA β-gal assay at the aortic root of *Apoe*$^{-/-}$ mice with western diet for 8 weeks (upper panel). SPiDer β-gal assay with Oct4 immunostaining (bottom panels) at the aortic roots. n = 5 mice/group.

Data are presented as mean ± SEM.

Stress granule formation is an important cellular process to stabilize mRNAs under various stress conditions. Many RNA-binding proteins, such as TDP-43 and hnRNPs, are aggregated with RNAs to prevent a stress-induced breakage and function as a storage for RNAs, which can cause re-initiation of gene expression (Guil et al., 2006; Hamilton et al., 1997; Henics et al., 1994). Based on recent studies demonstrating the regulation of Oct4 expression by hnRNP A2 in stem cells (Choi et al., 2013), we have tested that whether β-HB can modulate the binding affinity of hnRNP A1 with Oct4 mRNA in vascular cells. Our results show that the interaction of β-HB with hnRNP A1 enables hnRNP A1 to form a complex with Oct4 mRNA, resulting in stabilization of Oct4 mRNA *in vitro*.

Our second important finding is the functional role of Oct4 in adult somatic cells, specifically vascular tissues. Oct4 activation induced by β-HB strongly triggers quiescent vascular tissue via upregulating p21. As a result of Oct4 activation by β-HB under caloric restriction, increased cell quiescence markers such as mTOR inhibition, AMPK activation, Lamin B1 elevation, and low transcriptional activity were observed, while decreased senescence indictors such as induction of γH2AX, SASP expression, and SA β-gal activity were noted. Although previous studies have concluded that Oct4 is permanently silenced in adult somatic cells (Buganim et al., 2013; Cherepanova et al., 2016), the role of Oct4 should be reconsidered because it can be reactivated in certain adult somatic cells. Our results, along with recent reports, support Oct4 reactivation, contrary to previous dogma. Recent evidence shows that DNA demethylation can be a mechanism of Oct4 activation (Cherepanova et al., 2016; Kellner and Kikyo, 2010). Our results suggest another possibility for Oct4 activation via hnRNP A1-mediated stabilization of Oct4 mRNA in normal and oxidative stress condition.

We have demonstrated that the vascular cell quiescence triggered by β-HB and hnRNP A1-mediated Oct4 activation exhibits strong oxidative stress resistance and protects against cellular senescence. Cellular quiescence is a crucial process for maintaining the stemness of embryonic stem cells (ESCs) through inducing autophagy. We did not show sufficient results to prove β-HB induces autophagy and autophagy-dependent cellular quiescence (An et al., 2014; García-Prat et al., 2016). However, we predict that β-HB can induce autophagy in vascular cells, as well as ESCs, based on our observations of AMPK activation and mTOR inhibition by Oct4 upregulation after treating with β-HB in vascular cells. Future study will explore this hypothesis.

Interestingly, the anti-senescence effect of β-HB is exhibited more drastically in young cells. These observations can be explained when considering passage-dependent reduction of Oct4 mRNA. Knowing that the mechanism of β-HB-induced Oct4 elevation is via enhanced stability of Oct4 mRNA, the function of β-HB is limited in the total absence of any mRNA. Therefore, we assume that the anti-senescence effect of β-HB will not occur when aging is progressed or in case of Oct4 genetic deletion. Additionally, as shown in Figure 2, β-HB or serum deprivation promoted cell senescence in p53 hyper-activated cells stimulated by Nutlin-3a. Further studies are required to validate the role of β-HB in p53-dependent senescence or aging *in vivo* and *in vitro*.

Considering that aging is the most important non-modifiable risk factors for CVD and delaying or preventing vascular aging can protect again cardiovascular dysfunction, our study is significant because ketone body, produced during calorie restriction, delays vascular aging by preventing both replicative- and stress-induced senescence in vascular cells. This prevention of senescence by β-HB is via its direct binding of hnRNP A1, resulting in the stabilization of Oct4A mRNA and Oct4A expression. Targeting Oct4A by β-HB or β-HB-like compounds might be effective in preventing the occurrences or delaying the progression of CVD.

In summary, our studies reveal an important role for β-HB in cellular anti-senescence mediated by Oct4 upregulation in the vasculature system. It provides novel strategy to prevent senescence-associated vascular aging via accumulating or maintaining quiescent vascular cells. Thus, our research identifies Oct4 as a potent therapeutic target and β-HB and S-β-HB as a potent treatment for anti-aging or age-related vascular diseases.

STAR★METHODS

Detailed methods are provided in the online version of this paper and include the following:

- KEY RESOURCES TABLE
- CONTACT FOR REAGENT AND RESOURCE SHARING
- EXPERIMENTAL MODEL AND SUBJECT DETAILS
  - Cell Culture and Maintenance
  - Mice strains
  - Mouse model of atherosclerosis
- METHOD DETAILS
  - SA β-galactosidase assay
  - Fluorescein Di-β-D-Galactopyranoside assay (FDG)
  - SPiDer β-galactosidase assay
  - Synthesis of β-HB, Butyrate-conjugated beads, and S-β-HB salt
  - Affinity chromatography
  - Real-time RT-PCR
  - Immunofluorescence staining
  - Western blotting
  - Subcellular fractionation
  - RNA-immunoprecipitation (RIP)
  - Cell cycle analysis
  - Oct4 knockdown by CRISPR-Cas9
  - Primary aortic smooth muscle cell isolation
- QUANTIFICATION AND STATISTICAL ANALYSIS
- DATA AND SOFTWARE AVAILABILITY

SUPPLEMENTAL INFORMATION

Supplemental Information includes seven figures and can be found with this article at https://doi.org/10.1016/j.molcel.2018.07.036.

ACKNOWLEDGMENTS

This study was supported by the National Institutes of Health grants (HL079584, HL080499, HL089920, HL110488, HL128014, HL132500, HL137371, HL140954, HL142287, AG047776, and CA213022). This work was, in part, supported by the Georgia Research Alliance. M.-H.Z. is a Georgia Research Alliance Eminent Scholar in Molecular Medicine.

AUTHOR CONTRIBUTIONS

Y.-m.H. performed the all *in vitro* experiments. Y.-m.H. and T.B. performed all *in vivo* experiments. Y.-m.H. and P.S. analyzed the data and wrote the manuscript. Y.-m.H. and B.K.S. performed proteomics. Y.D. provided 64-week- and 96-week-old mice serum. Q.W. and Q.L. provided 64-week-old mice aorta tissues. M.-H.Z. conceived and designed the experiments, analyzed the data, and revised the manuscript.

DECLARATION OF INTERESTS

The authors declare no competing interests.

Received: October 9, 2017
Revised: April 2, 2018
Accepted: July 24, 2018
Published: September 6, 2018

REFERENCES

An, Z., Tassa, A., Thomas, C., Zhong, R., Xiao, G., Fotedar, R., Tu, B.P., Klionsky, D.J., and Levine, B. (2014). Autophagy is required for G_1/G_0 quiescence in response to nitrogen starvation in Saccharomyces cerevisiae. Autophagy *10*, 1702–1711.

Anton, S.D., Karabetian, C., Heekin, K., and Leeuwenburgh, C. (2013). Caloric restriction to moderate senescence: mechanisms and clinical utility. Curr. Transl. Geriatr. Exp. Gerontol. Rep. *2*, 239–246.

Bredesen, D.E., Amos, E.C., Canick, J., Ackerley, M., Raji, C., Fiala, M., and Ahdidan, J. (2016). Reversal of cognitive decline in Alzheimer's disease. Aging (Albany NY) *8*, 1250–1258.

Buganim, Y., Faddah, D.A., and Jaenisch, R. (2013). Mechanisms and models of somatic cell reprogramming. Nat. Rev. Genet. *14*, 427–439.

Cai, J., Weiss, M.L., and Rao, M.S. (2004). In search of "stemness." Exp. Hematol. *32*, 585–598.

Cherepanova, O.A., Gomez, D., Shankman, L.S., Swiatlowska, P., Williams, J., Sarmento, O.F., Alencar, G.F., Hess, D.L., Bevard, M.H., Greene, E.S., et al. (2016). Activation of the pluripotency factor OCT4 in smooth muscle cells is atheroprotective. Nat. Med. *22*, 657–665.

Cheung, T.H., and Rando, T.A. (2013). Molecular regulation of stem cell quiescence. Nat. Rev. Mol. Cell Biol. *14*, 329–340.

Childs, B.G., Durik, M., Baker, D.J., and van Deursen, J.M. (2015). Cellular senescence in aging and age-related disease: from mechanisms to therapy. Nat. Med. *21*, 1424–1435.

Childs, B.G., Baker, D.J., Wijshake, T., Conover, C.A., Campisi, J., and van Deursen, J.M. (2016). Senescent intimal foam cells are deleterious at all stages of atherosclerosis. Science *354*, 472–477.

Choi, H.S., Lee, H.M., Jang, Y.J., Kim, C.H., and Ryu, C.J. (2013). Heterogeneous nuclear ribonucleoprotein A2/B1 regulates the self-renewal and pluripotency of human embryonic stem cells via the control of the G1/S transition. Stem Cells *31*, 2647–2658.

Collado, M., and Serrano, M. (2010). Senescence in tumours: evidence from mice and humans. Nat. Rev. Cancer *10*, 51–57.

Colman, R.J., Beasley, T.M., Kemnitz, J.W., Johnson, S.C., Weindruch, R., and Anderson, R.M. (2014). Caloric restriction reduces age-related and all-cause mortality in rhesus monkeys. Nat. Commun. *5*, 3557.

Costantino, S., Paneni, F., and Cosentino, F. (2016). Ageing, metabolism and cardiovascular disease. J. Physiol. *594*, 2061–2073.

Finkel, T., Serrano, M., and Blasco, M.A. (2007). The common biology of cancer and ageing. Nature *448*, 767–774.

García-Prat, L., Martínez-Vicente, M., Perdiguero, E., Ortet, L., Rodríguez-Ubreva, J., Rebollo, E., Ruiz-Bonilla, V., Gutarra, S., Ballestar, E., Serrano, A.L., et al. (2016). Autophagy maintains stemness by preventing senescence. Nature *529*, 37–42.

Guil, S., Long, J.C., and Cáceres, J.F. (2006). hnRNP A1 relocalization to the stress granules reflects a role in the stress response. Mol. Cell. Biol. *26*, 5744–5758.

Hamilton, B.J., Burns, C.M., Nichols, R.C., and Rigby, W.F. (1997). Modulation of AUUUA response element binding by heterogeneous nuclear ribonucleoprotein A1 in human T lymphocytes. The roles of cytoplasmic location, transcription, and phosphorylation. J. Biol. Chem. *272*, 28732–28741.

Henics, T., Sanfridson, A., Hamilton, B.J., Nagy, E., and Rigby, W.F. (1994). Enhanced stability of interleukin-2 mRNA in MLA 144 cells. Possible role of cytoplasmic AU-rich sequence-binding proteins. J. Biol. Chem. *269*, 5377–5383.

Ito, K., Sportoletti, P., Clohessy, J.G., Silvia, G., and Pandolfi, P.P. (2010). The role of nucleophosmin in hematopoietic stem cells and the pathogenesis of myelodysplastic syndrome. Blood *116*, 48.

Jean-Philippe, J., Paz, S., and Caputi, M. (2013). hnRNP A1: the Swiss army knife of gene expression. Int. J. Mol. Sci. *14*, 18999–19024.

Kellner, S., and Kikyo, N. (2010). Transcriptional regulation of the Oct4 gene, a master gene for pluripotency. Histol. Histopathol. *25*, 405–412.

Kim, K.H., Chen, C.C., Monzon, R.I., and Lau, L.F. (2013). Matricellular protein CCN1 promotes regression of liver fibrosis through induction of cellular senescence in hepatic myofibroblasts. Mol. Cell. Biol. *33*, 2078–2090.

Kovacic, J.C., Moreno, P., Hachinski, V., Nabel, E.G., and Fuster, V. (2011). Cellular senescence, vascular disease, and aging: Part 1 of a 2-part review. Circulation *123*, 1650–1660.

Lengner, C.J., Welstead, G.G., and Jaenisch, R. (2008). The pluripotency regulator Oct4: a role in somatic stem cells? Cell Cycle *7*, 725–728.

Liu, R., Liu, H., Ha, Y., Tilton, R.G., and Zhang, W. (2014). Oxidative stress induces endothelial cell senescence via downregulation of Sirt6. BioMed Res. Int. *2014*, 902842.

Martin, B., Mattson, M.P., and Maudsley, S. (2006). Caloric restriction and intermittent fasting: two potential diets for successful brain aging. Ageing Res. Rev. *5*, 332–353.

Martin, C., Chen, S., Maya-Mendoza, A., Lovric, J., Sims, P.F., and Jackson, D.A. (2009). Lamin B1 maintains the functional plasticity of nucleoli. J. Cell Sci. *122*, 1551–1562.

Minamino, T., and Komuro, I. (2007). Vascular cell senescence: contribution to atherosclerosis. Circ. Res. *100*, 15–26.

Minor, R.K., Allard, J.S., Younts, C.M., Ward, T.M., and de Cabo, R. (2010). Dietary interventions to extend life span and health span based on calorie restriction. J. Gerontol. A Biol. Sci. Med. Sci. *65*, 695–703.

Ning, Y.C., Cai, G.Y., Zhuo, L., Gao, J.J., Dong, D., Cui, S., Feng, Z., Shi, S.Z., Bai, X.Y., Sun, X.F., and Chen, X.M. (2013). Short-term calorie restriction protects against renal senescence of aged rats by increasing autophagic activity and reducing oxidative damage. Mech. Ageing Dev. *134*, 570–579.

North, B.J., and Sinclair, D.A. (2012). The intersection between aging and cardiovascular disease. Circ. Res. *110*, 1097–1108.

Paoli, A., Bianco, A., Damiani, E., and Bosco, G. (2014). Ketogenic diet in neuromuscular and neurodegenerative diseases. BioMed Res. Int. *2014*, 474296.

Sadaie, M., Dillon, C., Narita, M., Young, A.R., Cairney, C.J., Godwin, L.S., Torrance, C.J., Bennett, D.C., Keith, W.N., and Narita, M. (2015). Cell-based screen for altered nuclear phenotypes reveals senescence progression in polyploid cells after Aurora kinase B inhibition. Mol. Biol. Cell *26*, 2971–2985.

Saldivia, M., Ceballos-Pérez, G., Bart, J.M., and Navarro, M. (2016). The AMPKα1 Pathway Positively Regulates the Developmental Transition from Proliferation to Quiescence in Trypanosoma brucei. Cell Rep. *17*, 660–670.

Salmenperä, P., Karhemo, P.R., Räsänen, K., Laakkonen, P., and Vaheri, A. (2016). Fibroblast spheroids as a model to study sustained fibroblast quiescence and their crosstalk with tumor cells. Exp. Cell Res. *345*, 17–24.

Shimi, T., Butin-Israeli, V., Adam, S.A., Hamanaka, R.B., Goldman, A.E., Lucas, C.A., Shumaker, D.K., Kosak, S.T., Chandel, N.S., and Goldman,

R.D. (2011). The role of nuclear lamin B1 in cell proliferation and senescence. Genes Dev. *25*, 2579–2593.

Spring, D.R. (2005). Chemical genetics to chemical genomics: small molecules offer big insights. Chem. Soc. Rev. *34*, 472–482.

Stone, G.W., Lansky, A.J., Pocock, S.J., Gersh, B.J., Dangas, G., Wong, S.C., Witzenbichler, B., Guagliumi, G., Peruga, J.Z., Brodie, B.R., et al.; HORIZONS-AMI Trial Investigators (2009). Paclitaxel-eluting stents versus bare-metal stents in acute myocardial infarction. N. Engl. J. Med. *360*, 1946–1959.

Takahashi, K., and Yamanaka, S. (2006). Induction of pluripotent stem cells from mouse embryonic and adult fibroblast cultures by defined factors. Cell *126*, 663–676.

Tchkonia, T., Zhu, Y., van Deursen, J., Campisi, J., and Kirkland, J.L. (2013). Cellular senescence and the senescent secretory phenotype: therapeutic opportunities. J. Clin. Invest. *123*, 966–972.

Tian, X.L., and Li, Y. (2014). Endothelial cell senescence and age-related vascular diseases. J. Genet. Genomics *41*, 485–495.

Tieu, K., Perier, C., Caspersen, C., Teismann, P., Wu, D.C., Yan, S.D., Naini, A., Vila, M., Jackson-Lewis, V., Ramasamy, R., and Przedborski, S. (2003). D-beta-hydroxybutyrate rescues mitochondrial respiration and mitigates features of Parkinson disease. J. Clin. Invest. *112*, 892–901.

Uryga, A.K., and Bennett, M.R. (2016). Ageing induced vascular smooth muscle cell senescence in atherosclerosis. J. Physiol. *594*, 2115–2124.

van Deursen, J.M. (2014). The role of senescent cells in ageing. Nature *509*, 439–446.

Wang, J.C., and Bennett, M. (2012). Aging and atherosclerosis: mechanisms, functional consequences, and potential therapeutics for cellular senescence. Circ. Res. *111*, 245–259.

Will, B., Vogler, T.O., Bartholdy, B., Garrett-Bakelman, F., Mayer, J., Barreyro, L., Pandolfi, A., Todorova, T.I., Okoye-Okafor, U.C., Stanley, R.F., et al. (2013). Satb1 regulates the self-renewal of hematopoietic stem cells by promoting quiescence and repressing differentiation commitment. Nat. Immunol. *14*, 437–445.

Williams, A.B., and Schumacher, B. (2016). p53 in the DNA-damage-repair process. Cold Spring Harb. Perspect. Med. *6*, a026070.

Wu, J., Lu, L.Y., and Yu, X. (2010). The role of BRCA1 in DNA damage response. Protein Cell *1*, 117–123.

Xu, H., Zhou, Y., Coughlan, K.A., Ding, Y., Wang, S., Wu, Y., Song, P., and Zou, M.H. (2015). AMPKα1 deficiency promotes cellular proliferation and DNA damage via p21 reduction in mouse embryonic fibroblasts. Biochim. Biophys. Acta *1853*, 65–73.

Yarden, R.I., Pardo-Reoyo, S., Sgagias, M., Cowan, K.H., and Brody, L.C. (2002). BRCA1 regulates the G2/M checkpoint by activating Chk1 kinase upon DNA damage. Nat. Genet. *30*, 285–289.

Zhu, Y., Armstrong, J.L., Tchkonia, T., and Kirkland, J.L. (2014). Cellular senescence and the senescent secretory phenotype in age-related chronic diseases. Curr. Opin. Clin. Nutr. Metab. Care *17*, 324–328.

STAR★METHODS

KEY RESOURCES TABLE

REAGENT or RESOURCE	SOURCE	IDENTIFIER
Antibodies		
Rabbit polyclonal anti-p16	Abcam	Cat#ab189034; RRID: AB_2737282
Rabbit polyclonal anti-p21	Cell Signaling	Cat#2947S; RRID: AB_823586
Rabbit polyclonal anti-p27	Cell Signaling	Cat#2552S; RRID: AB_10693314
Rabbit polyclonal anti-p53	Cell Signaling	Cat#9282S; RRID: AB_10693944
Rabbit monoclonal anti-Oct4A	Thermo Fisher	Cat#A13998; RRID: AB_2534182
Rabbit monoclonal anti-Oct4-FITC	NOVUS	Cat#NB100-2379F; RRID: AB_2737283
Rabbit polyclonal anti-Lamin B1	Cell Signaling	Cat#12586S; RRID: AB_2534182
Rabbit polyclonal anti-Lamin A/C	Cell Signaling	Cat#2032S; RRID: AB_2136278
Rabbit polyclonal anti-hnRNP A1	Cell Signaling	Cat#8443S; RRID: AB_10828725
Rabbit monoclonal anti-NPM1	Thermo Fisher	Cat#MA5-12508; RRID: AB_10981922
Rabbit polyclonal anti-IL-6	Cell Signaling	Cat#12153S; RRID: AB_2687897
Rabbit polyclonal anti-γH2AX	Cell Signaling	Cat#2577S; RRID: AB_2118010
Rabbit polyclonal anti-p-CHK1 (S345)	Cell Signaling	Cat#2348S; RRID: AB_331212
Rabbit polyclonal anti-p-BRCA1 (S1524)	Cell Signaling	Cat#9009S; RRID: AB_491003
Rabbit polyclonal anti-p-RB (S780)	Cell Signaling	Cat#9307S; RRID: AB_330015
Rabbit polyclonal anti-p-RB (S807, S811)	Cell Signaling	Cat#9308S; RRID: AB_331472
Rabbit polyclonal anti-p-P70 (T389)	Cell Signaling	Cat#9205S; RRID: AB_330944
Rabbit polyclonal anti-eIF4E	Cell Signaling	Cat#9742S; RRID: AB_823488
Rabbit polyclonal anti-TIA-1	Santa Cruz Bio	Cat#SC-166247; RRID: AB_2201545
Rat monoclonal anti-CD31	Abcam	Cat#ab56299; RRID: AB_940884
Mouse monoclonal anti-α-smooth muscle actin	Abcam	Cat#ab7817; RRID: AB_262054
Mouse monoclonal anti-β-Actin	Santa Cruz Bio	Cat#SC-47778; RRID: AB_2714189
Mouse monoclonal anti-α-Tubulin	Cell Signaling	Cat#3873S; RRID: AB_1904178
Chemicals, Peptides, and Recombinant Proteins		
(R)-3-Hydroxybutyric acid	Sigma-Aldrich	54920; CAS: 625-72-9
(S)-3-Hydroxybutyric acid	Sigma-Aldrich	54925**; CAS: 6168-83-8**
Litium acetoacetate	Sigma-Aldrich	A8509; CAS: 3483-11-2
Sodium butyrate	Sigma-Aldrich	303410; CAS: 156-54-7
Hydrogene Peroxide	Fisher Scientific	H325-500; CAS: 7722-84-1
Propidium iodide	Sigma-Aldrich	P4170; CAS: 25535-16-4
Aphidicolin	Sigma-Aldrich	A0781; CAS: 38966-21-1
Nutlin-3a	Sigma-Aldrich	SML0580; CAS: 675576-98-4
Actinomycin D	Sigma-Aldrich	A1410; CAS: 50-76-0
NHS-Activated Sepharose 4 Fast Flow	GE Healthcare	Cat#17090601
(S)-(+)-4-Amino-3-hydroxybutyric acid	Sigma-Aldrich	542946; CAS: 7013-05-0
γ-Aminobutyric acid	Sigma-Aldrich	A2129; CAS: 56-12-2
Ethyl (R)-(-)-3-hydroxybutyrate	Sigma-Aldrich	347329; CAS: 24915-95-5
Protein A/G Magnetic Beads	Thermo Fisher	Cat#88802
Fluorescein Di-β-D-Galactopyranoside (FDG)	Thermo Fisher	F1179; CAS: 17817-20-8
SPiDer-β-Gal	Dojindo	SG02-10; CAS: 1824699-57-1
Sucrose	Sigma-Aldrich	S1888; CAS: 57-50-1
Albumin, Bovine Fraction V (BSA)	RPI	A30075-100; CAS: 9048-46-8
Fetal bovine sereum (FBS)	Sigma-Aldrich	Cat#12303C

(*Continued on next page*)

Continued

REAGENT or RESOURCE	SOURCE	IDENTIFIER
Penicillin-Streptomycin	Thermo Fisher	15140122; CAS: 69-57-8
EBM basal Medium	Lonza	Cat#CC-3121
Media 231	GIBCO	Cat#M-231-500
DMEM/F12 medium	GIBCO	Cat#11320
Collagenase Type II	Worthington Biochemical	LS004174; CAS: 9001-12-1
Elastase	Worthington Biochemical	LS002279; CAS: 39445-21-1
EGM SingleQuat Kit Suppl. & Growth Factors	Lonza	Cat#CC-4133
Smooth Muscle Growth Supplement (SMGS)	Thermo Fisher	Cat#S00725
Critical Commercial Assays		
Senescence β-Galactosidase Staining Kit	Cell Signaling	9860
Fluorescein Di-β-D-Galactopyranoside	Invitrogen	F1179
SPiDer β- galactosidase assay	Dojindo	SG02-10
iScript cDNA Synthesis Kit	Bio-Rad	1708890
β-Hydroxybutyrate Colorimetric Assay Kit	BioVision	K632
Annexin-V-FLUOS Staining Kit	Cell Signaling	11988549001
Mouse IL-6 ELISA MAX Deluxe	BioLegend	431306
Mouse IL-1α ELISA MAX Deluxe	BioLegend	433406
Experimental Models: Cell Lines		
Human: Umbilical Vein Endo Cells (HUVECs)	Thermo Fisher	LSC0035C
Human: Aortic Smooth Muscle Cells (hASMCs)	Thermo Fisher	C0075C
Experimental Models: Organisms/Strains		
Mouse: C57BL/6J (3 weeks)	The Jackson Lab	JAX000664; RRID: IMSR_JAX:000664
Mouse: Aged C57BL/6J (64 weeks)	The Jackson Lab	JAX000664; RRID: IMSR_JAX:000664
Recombinant DNA		
pSpCas9(BB)-2A-GFP (PX458)	Addgene	Cat#48138
CRISPR/Cas9-Oct4	This paper	N/A
Oct4-myc	This paper	N/A
Software and Algorithms		
GraphPad Prism 5	GraphPad Software	https://www.graphpad.com/
ImageJ Software	ImageJ	http://imagej.net/
ChemBio Ultra 14.0	PerkinElmer	http://www.cambridgesoft.com
Zen	ZEISS Microscope	https://www.zeiss.com/corporate/int/home.html
FlowJo	FlowJo LLC	
Deposited data	This paper	https://doi.org/10.17632/t57mvdfz39.1

CONTACT FOR REAGENT AND RESOURCE SHARING

Further information and requests for reagents may be directed to the Lead Contact, Ming-Hui Zou (mzou@gsu.edu).

EXPERIMENTAL MODEL AND SUBJECT DETAILS

Cell Culture and Maintenance

Human umbilical vein endothelial cells (HUVECs, catalog no. LSC0035C) and human aortic smooth muscle cells (hASMCs, catalog no. C0075C), isolated from an individual donor were originally obtained from the Thermo Fisher Scientific (Waltham, MA, USA). HUVECs were cultured in EBM Basal Medium (Lonza, catalog no. CC-3121) supplemented with EGM SingleQuats (Lonza, catalog no. CC-4133) and hASMCs were cultured in Medium 231 (GIBCO, catalog no. M231500) supplemented with SMGS (GIBCO, catalog no. S00725). All culture media were supplemented with 5% heat-inactivated fetal bovine serum (FBS, GIBCO), 100 U mL^{-1} penicillin, and 0.1 mg mL^{-1} streptomycin (Sigma-Aldrich) in a 37°C incubator with humidity and 5% CO_2. HUVECs and hASMCs were obtained from single donor. And mice primary cells were isolated from 6 mice/group at the same day. The cells were maintained and regularly tested for mycoplasma contamination by PCR and confirmed to be free of any contamination.

Mice strains

C57BL/6J mice were purchased from the Jackson Laboratory. All mice were housed in temperature-controlled rooms with a 12 h light-dark cycle and given free access to water and food. After starvation for 5 h, 8 weeks-old male mice were injected intraperitoneally with PBS, β-HB, or S-β-HB (1.5 g/kg body weight in PBS). In parallel, 8 weeks-old male mice were randomized and fed a regular chow diet or fasted for 72 h. Then, the mice were sacrificed. Tissues were collected for gene expression evaluation in various organs including the aorta, liver, heart, brain, adipose, and kidney (n = 6). All animal protocols were reviewed and approved by the Institutional Animal Care and Use Committee at Georgia State University.

Mouse model of atherosclerosis

8 weeks old male Apoe−/− mice (n = 10) were fed a western diet (21% milk fat, 0.15% cholesterol) for 8 weeks to establish aortic lesions. Mice aortic roots were fixed overnight in 4% paraformaldehyde, then embedded in optimum cutting temperature compound (OCT).

METHOD DETAILS

SA β-galactosidase assay

SA β-gal staining kit (Cell Signaling Technology, catalog no. 9860) was used to stain senescent cells. According to the manufacturer's instructions (Cell Signaling Technology), HUVECs and hASMCs were fixed for 10 min, stained for 1 day and analyzed. Senescent cells, identified as blue-stained cells, were captured with light microscopy (Olympus IX73), then images were processed using imaging software (CellSens Dimension). Mice aortas were fixed for 10 min, stained for 1week and captured with light microscopy.

Fluorescein Di-β-D-Galactopyranoside assay (FDG)

Fluorescein Di-β-D-Galactopyranoside (FDG) was used to quantify the SA β-gal activity in HUVECs. FDG was dissolved in DMSO solution in which the sock solution (FDG, 200 mM) was stored at −20°C. Cells were cultured in 96-well plates, washed with PBS, then fixed with solution (2% formaldehyde, 0.2% glutaraldehyde). Staining solution (37 mM citric acid, 126 mM Na_2HPO_4, 5 mM potassium ferricyanide, 5 mM potassium ferrocyanide, 150 mM NaCl, 2 mM $MgCl_2$) was added to each well, then 10 μL of 2 mM FDG was added to each well. After incubation in the dark at 37°C for 24 h without CO_2 supply, the supernatant was transferred to a 96-well plate and fluorescein fluorescence was measured using the fluorometer (Tecan M1000) with a 485 nm excitation and a 535 nm emission wavelength. Genomic DNA of attached cells was measured with Qubit dsDNA HS assay kit in order to normalize β-galactosidase activity.

SPiDer β-galactosidase assay

Cells were washed with PBS, and SPiDer β-Gal working solution was added to the culture dish for 30 min at 37°C. After reaction, cells were washed with PBS, then fixed with 4% PFA/PBS solution. SA β-galactosidase positive cells were captured under fluorescence microscope with a 488 nm excitation and 533 nm emission wavelength. The mice aortas were separated into aortic arch and thoracic aorta to performed SPiDer β-gal assay. Aortic arch and thoracic aorta were embedded in optimum cutting temperature compound (OCT) compound. Then, 2.5 mm of aortic arch was sectioned every 0.5 mm from innominate artery to left subclavian, and 5 mm of thoracic aorta was sectioned every 1 mm from the middle portion of the descending thoracic aorta to diaphragm. Tissue slides were washed with PBS, and reacted by SPiDer β-gal solution for one hour at 37°C. After washing slides with PBS, SA β-galactosidase positive areas were captured under fluorescence microscope with a 488 nm excitation and 533 nm emission wavelength.

Synthesis of β-HB, Butyrate-conjugated beads, and S-β-HB salt

(*S*)-(+)-4-Amino-3-hydroxybutyric acid was dissolved in coupling buffer (0.2 M $NaHCO_3$, 0.5 M NaCl, pH 8.3), and prewashed NHS-activated Sepharose beads (10 mL) were added to the solution. The mixture was incubated in a 4°C shaker for 24 h. Then, the remaining NHS-activated groups were blocked with blocking buffer (0.5 M ethanolamine, 0.5 M NaCl, pH 8.3). β-HB and Butyrate-conjugated beads were washed with washing buffer (0.1 M Tris-HCl, pH 8.9). In order to prepare S-β-HB salt, (*S*)-hydroxybutyric acid was dissolved in acetone, then 0.1 mM of NaOH solution was added dropwise. Crystalized white power was washed by acetone and dried. ^{1}H NMR (D_2O): δ 4.07 (m, 1H), 2.33 (t, 1H), 2.21 (t, 1H), 1.12 (d, 3H).

Affinity chromatography

Cultured HUVECs were washed with PBS and then homogenized with a 26-gauge syringe in binding buffer (10 mM Tris-HCl, pH 7.4, 50 mM KCl, 5 mM $MgCl_2$, 1 mM EDTA, and 0.1 mM Na_3VO_4). The cell lysate was centrifuged at 13,000 rpm for 20 min at 4°C, and the supernatant was collected. In total, 4 mg of protein was obtained. The cell lysate was precleared by incubation with non-conjugated Sepharose beads and then loaded into a 15 mL volume of β-HB or Butyrate-conjugated Sepharose beads. After washing with 3 volumes of washing buffer (0.1 M Tris-HCl, pH 8.9), affinity chromatography was performed with β-HB gradient elution buffer (0.1 M Tris-HCl, β-HB 0.5 mM–8 mM). Samples were concentrated and separated by SDS-PAGE and visualized by Coomassie Brilliant Blue staining. The samples were then digested with trypsin, and peptide tandem mass spectrometry analysis of the digested peptides was performed using a Matrix-assisted laser desorption/ionization (MALDI) time-of-flight mass spectrometer.

Real-time RT-PCR

Total RNA was isolated using the RNeasy Mini Kit (QIAGEN, Cat no. 74106) and purified according to the manufacturer's instruction. Synthesis of cDNA was conducted using iScript cDNA Synthesis Kit (Bio-Rad, Cat no. 1708890) according to the manufacturer's instruction. Gene expression was quantified with the CFX96 real-time system (Bio-Rad) using the iQ SYBR Green supermix (Bio-Rad). The relative amounts of each mRNA were calculated by the comparative ΔC_t method using GAPDH as house-keeping genes. Relative expression was calculated using the cycling threshold (C_t) method as $2^{-\Delta Ct}$.

Primer	Forward (5′ to 3′)	Reverse (5′ to 3′)
Oct4A	CGTGAAGCTGGAGAAGGAGAAGCTG	CAAGGGCCGCAGCTTACACATGTTC
Oct4B	ATGCATGAGTCAGTG AACAG	CCACATCGGCCTGTGTATAT
IL-1α	ATCAGTACCTCACGGCTGCT	TGGGTATCTCAGGCATCTCC
IL-6	CCAGCTATGAACTCCTTCTC	GCTTGTTCCTCACATCTCTC
IL-8	ATGACTTCCAAGCTGGCCGTGGCT	TCTCAGCCCTCTTCAAAAACTTCTC
SOX2	GGGAAATGGGAGGGGTGCAAAAGAGG	TTGCGTGAGTGTGGATGGGATTGGTG
KLF4	GTTTTGAGGAAGTGCTGAG	CAGTCACAGTGGTAAGGTTT
c-Myc	GTTGGTCAGGCTGGTCTTGAA	CATGCGCCTGTAATCCTAGCA
Nanog	ACCAGAACTGTGTTCTCTTCCACC	GGTTGCTCCAGGTTGAATTGTTCC
GAPDH	CAACTTTGGCATTGTGGAAGG	ACACATTGGGG GTAGGAACAC

Immunofluorescence staining

After β-HB treatment to the HUVECs, hASMCs or prepared thoracic aorta tissue of mice, samples were fixed with 4% paraformaldehyde (v/v) in PBS for 12 min at room temperature (RT), permeabilized with 0.2% Triton X-100 (v/v) in PBS for 10 min at RT, and blocked with 5% normal goat serum for 30 min at RT. Cells were incubated with primary antibodies (1: 500) at 37°C for 30 min, then followed by Alexa Fluor® 488 or 647 conjugated secondary antibodies (1: 500) at 37°C for 60 min. Images were captured using confocal microscope or fluorescence microscope.

Western blotting

Cell lysates were prepared in RIPA lysis buffer (50 mM Tris, pH 7.0, 150 mM NaCl, 5 mM EDTA, 1% deoxycholic acid, 0.1% SDS, 30 mM Na_2HPO_4, 50 mM NaF, and 1 mM $NaVO_4$) containing protease inhibitor cocktail (Roche Applied Science). Proteins (40 μg) were resolved by 8 or 12% SDS-PAGE and transferred to PVDF membranes (Millipore). The membrane was blocked with 5% nonfat dry milk in TBS-T (50 mM Tris-HCl, pH 7.6, 150 mM NaCl, and 0.1% Tween-20) and probed with primary antibodies overnight at 4°C. The secondary antibodies used were horseradish peroxidase-conjugated goat anti-rabbit or anti-mouse IgG (Cell Signaling Technology). The membranes were washed 3 times with TBS-T and then visualized with chemiluminescent peroxidase reagents (Roche, Germany).

Subcellular fractionation

Cells were harvested and homogenized by pass through a 27 gauge needle 10-times with fractionation buffer (150 mM KCl, 25 mM Tris pH 7.4, 5 mM EDTA, 0.5 mM, protease inhibitors). Centrifuge the cell lysate at 800 × G for 10 min. The pellet contains nuclei proteins and the supernatant contains cytoplasmic, mitochondrial and plasma-membrane proteins. Centrifuge supernatant at 10,000 × G for 20min. The pellet contains mitochondrial proteins and the supernatant contains cytoplasmic and plasma-membrane proteins. Finally, Centrifuge supernatant at 100,000 × G for 1 h. The supernatant contains pure cytoplasmic proteins and the pellet contains plasma-membrane proteins.

RNA-immunoprecipitation (RIP)

Cytoplasmic proteins were obtained through subcellular fractionation method described in Method part. Cell lysate was resuspended in freshly prepared RIP buffer (150 mM KCl, 25 mM Tris pH 7.4, 5 mM EDTA, 0.5 mM DTT, 0.5% NP40, 100 U/mL RNAase inhibitor, and protease inhibitor). Antibodies to hnRNP A1 were added to supernatant and incubated for overnight at 4°C with gentle rotation. Protein A/G beads were added, then incubated for 2 h at 4°C with gentle rotation. Precipitated beads were washed three times and resuspended with RIP buffer. Bound RNAs were extracted with TRIzol according to manufacturer's instruction. Synthesis of cDNA was conducted using iScript cDNA Synthesis Kit according to the manufacturer's instruction. Gene expression was quantified on the CFX96 real-time system (Bio-Rad) using the iQ SYBR Green supermix (Bio-Rad).

Cell cycle analysis

HUVECs and hASMCs were trypsinized from the culture dish after β-HB treatment and gathered by centrifugation. Precipitated cells were washed twice by repeating suspension and precipitation in PBS buffer. Precipitated cells were suspended with 500 μL PBS and fixed with 5 mL of ice-cold 70% ethanol overnight. Fixed cells were harvested and resuspended in PBS and treated with 100 μg/mL of RNase A at 37°C for 20 min. Propidium iodide (PI) was then added at a final concentration of 50 μg/mL for DNA staining, and 10,000 fixed cells were analyzed on a FACS Fortessa (BD Biosciences). For G0 phase analysis, Pyronin Y and Hoechst 33342 were used to stain mRNA and DNA separately. Cells were harvested in the same manner as described above, then re-suspend in culture media containing 10 μg/mL Hoechst 33342, incubated at 37°C for 15 min, then 5 μL of 100 ug/mL Pyronin Y was added. After a 15 min incubation, cells were transferred to ice and 10,000 cells were analyzed on a FACS Fortessa (BD Biosciences).

Oct4 knockdown by CRISPR-Cas9

Oct4A knockout HUVECs were prepared by CRISPR-Cas9-mediated gene editing. We used CRISPR design tool (http://tools.genome-engineering.org) to select Oct4 target sequences. Potential target oligomers for sgRNA constructs was designed with high efficiency score. Oct4 sgRNA sequence was 5′-CACCGGCACTAGCCCCACTCCAACC-3′ and 5′-AAACGGTTGGAGTGGGGCTAGTGCC-3′. Oct4 targeting gRNA was inserted into PX459 plasmid, then HUVECs were transfected with this plasmid. After transfection, the cells were selected with medium containing 2.0 μg/mL Puromycin.

Primary aortic smooth muscle cell isolation

Mice aortas were prepared from 6 mice to obtain sufficient cells for flow cytometry analysis. Dissected aortas are rinsed with PBS and placed into a dish with enzyme solution (1 mg/ml Collagenase Type II, 0.744 units/ml Elastase, PBS) containing 1% of penicillin-streptomycin. After incubation at 37°C for 10 minutes, aortas are placed into dish with DMEM/F12 media. Adventitia is removed by forceps, then aortas are chopped and incubated at 37°C in 5% CO_2 incubator for 1 hour with enzyme solution. Chopped aortas are washed with media by centrifugation and placed into collagen coated plate. After 2 days, floating debris are removed by changing media, and cluster of primary cells were maintained up to two passages. 80% confluence of smooth muscle cells were fixed and analyzed by flow cytometry.

QUANTIFICATION AND STATISTICAL ANALYSIS

All experiments were performed at least three times and multiple samples represent biological replicates. All animal experiments were performed using randomly assigned mice. Statistical significance was tested using two-tailed Student's t test when the two group were compared. Statistical significance was tested using Two-way ANOVA with Bonferroni post hoc tests when multiple groups were compared. Values are the mean ± SE of three independent experiment. Values of $p < 0.05$, $p < 0.01$ and $p < 0.001$ are denoted by *, ** and *** or #, ##, ### respectively.

DATA AND SOFTWARE AVAILABILITY

The accession number for the original images reported in this paper is https://doi.org/10.17632/t57mvdfz39.1.

Molecular Cell, Volume *71*

Supplemental Information

β-Hydroxybutyrate Prevents Vascular Senescence through hnRNP A1-Mediated Upregulation of Oct4

Young-min Han, Tatiana Bedarida, Ye Ding, Brian K. Somba, Qiulun Lu, Qilong Wang, Ping Song, and Ming-Hui Zou

Supplemental Figures

Figure S1. Related to Figure 1

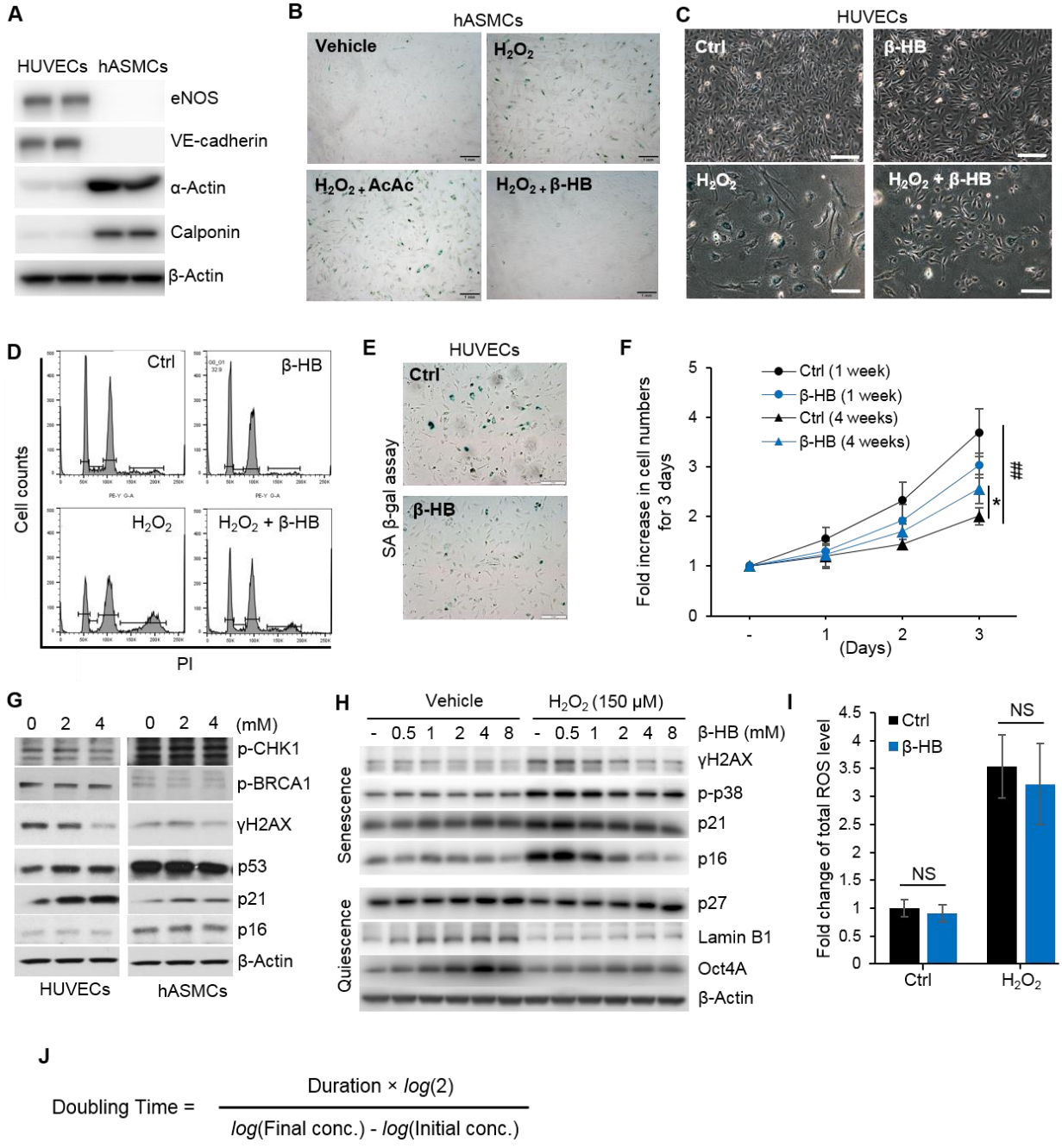

J

$$\text{Doubling Time} = \frac{\text{Duration} \times log(2)}{log(\text{Final conc.}) - log(\text{Initial conc.})}$$

Supplemental Figure 1 (related to Figure 1). Preventive effect of β-hydroxybutyrate (β-HB) on the cellular senescence.

(A) Western blots for endothelial cell markers (eNOS and VE-cadherin) and smooth muscle cell markers (α-Actin and Calponin) in the HUVECs and hASMCs. n = 2.

(B) Representative image of senescence-associated β-galactosidase (SA β-gal) activity assay of hASMCs after hydrogen peroxide (H_2O_2, 150 μM, 3 days) stimulation. Cells were co-treated with acetoacetate (AcAc, 4 mM) or β-hydroxybutyrate (β-HB, 4 mM) for 3 days. Scale bar, 100 μm. n = 3.

(C) Morphological change of HUVECs after H_2O_2 (150 μM, 3 days) stimulation. Cells were co-treated with or without β-HB (4 mM, 3 days). Scale bar, 100 μm. n = 3.

(D) Cell cycle distribution of HUVECs after β-HB (4 mM) treatment for 3 days with or without H_2O_2 (150 μM). Cells were analyzsed by flow cytometry after propidium iodide (PI) staining, based on 10,000 cells. n = 3

(E) Representative images of SA β-gal activity assay of HUVECs with or without β-HB treatment (4 mM) for 4 weeks. n = 3.

(F) HUVECs were maintained with or without β-HB (4 mM) treatment for 1 week or 4 weeks. After treatment, proliferation of HUVECs was analyzed by counting the cell numbers for 3 days. $^{*}p < 0.05$, Ctrl (4 weeks) *vs.* β-HB (4 weeks), $^{\#\#}p < 0.01$ Ctrl (1 week) *vs.* Ctrl (4 weeks). n = 3.

(G) Representative Western blots for DNA repair signaling (p-CHK1 and p-BRCA1), DNA damage (γH2AX) and cell cycle regulatory proteins (p53, p21 and p16) in HUVECs or hASMCs after β-HB treatment (2-4 mM). n = 3.

(H) Representative Western blots for senescence (γH2AX, p-p38, p21, and p16) and quiescence (p27, Lamin B1, and Oct4A) markers in hASMCs treated with or without β-HB for 24 h in a dose dependent manner. n = 3.

(I) DCFDA/H2DCFDA cellular reactive oxygen species (ROS) assay to measure total ROS level, stimulated by hydrogen peroxide (H_2O_2, 150 μM) with or without β-HB treatment (4 mM). NS, non-significant.

(J) Equation to calculate doubling time of HUVECs.

Data are presented as mean ± standard error of mean (SEM). NS, non-significant; Ctrl, control.

Figure S2 (related to Figure 2).

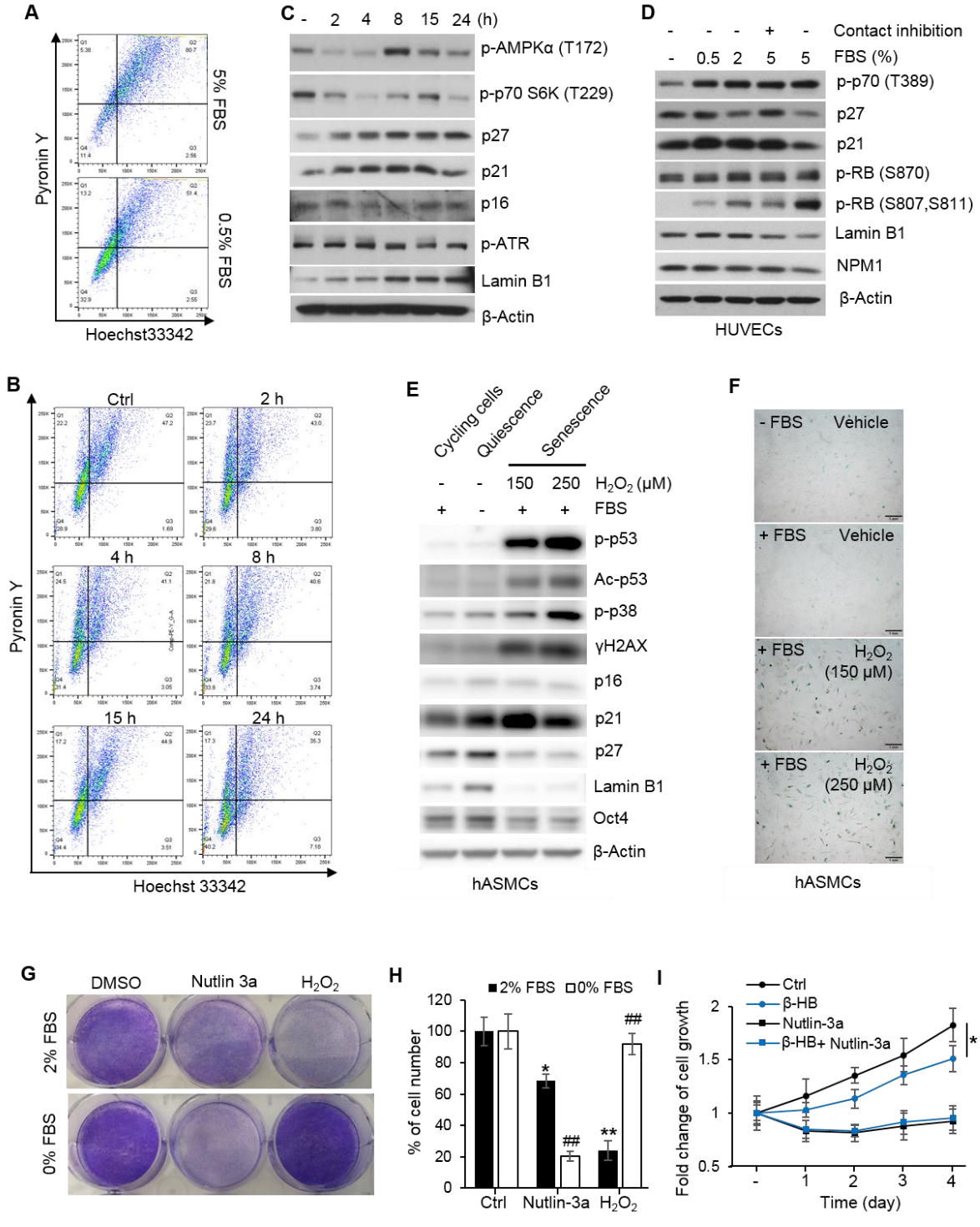

Supplemental Figure 2 (related to Figure 2). Induction of cellular quiescence in HUVECs by β-HB treatment.

(A) Cell cycle distribution of quiescent HUVECs (G0 phage) cultured with nutrient complete (5% FBS, EGF, bovine brain extract) or FBS-deprived media (0.5% FBS, EGF, bovine brain extract), assessed by flow cytometry analysis of the intercalation of Pyronin Y and Hoechst 33342. Each samples were analyzed based on 10,000 cells.

(B) Cell cycle distribution of HUVECs with time-dependent treatment of β-HB (2 h-24 h), assessed by flow cytometry analysis of the intercalation of Pyronin Y and Hoechst 33342. Samples were analyzed based on 10,000 cells.

(C) Representative Western blots for quiescence- or senescence-associated signaling proteins (p-AMPKa, p-p70 S6K, p27, p21, p16, p-ATR and Lamin B1) in HUVECs treated with β-HB (4 mM) in a time-dependent manner. n = 3.

(D) Representative Western blots for quiescence markers (p-p70, p27, p21, p-RB, Lamin B1 and NPM1), which were induced by contact inhibition or FBS deprivation in HUVECs. n = 3.

(E) Representative Western blots for quiescence (p27, Lamin B1 and Oct4) and senescence markers (p-p53, Ac-p53, p-p38, γH2AX, p16 and p21) in hASMCs. FBS deprivation-induced quiescent cells and H_2O_2 (150-250 μM, 24 h)-stimulated senescent cells were compared to cycling cells. n = 3.

(F) Representative images of SA β-gal activity assay in hASMCs, cultured with FBS deprivation (24 h) or H_2O_2 (150-250 μM, 24 h) treatment. n = 3.

(G) Representative images of crystal violet staining to exhibit the number of HUVECs after Nutlin-3a or H_2O_2 treatment in different conditioned media (2% FBS or 0% FBS). n = 3.

(H) Quantitation of Figure S2G. $^{*}p < 0.05$, $^{**}p < 0.01$ control *vs.* Nutlin-3a or H_2O_2, $^{\#\#}p < 0.01$ 2% FBS *vs.* 0% FBS, n = 3.

(I) Growth rate of HUVECs was analyzed by counting cell numbers every days after treating β-HB and Nutlin-3a. n = 3, $^{*}p < 0.05$ control (4 days) vs. β-HB (4 days).

Data are presented as mean ± standard error of mean (SEM).

Figure S3 (related to Figure 3).

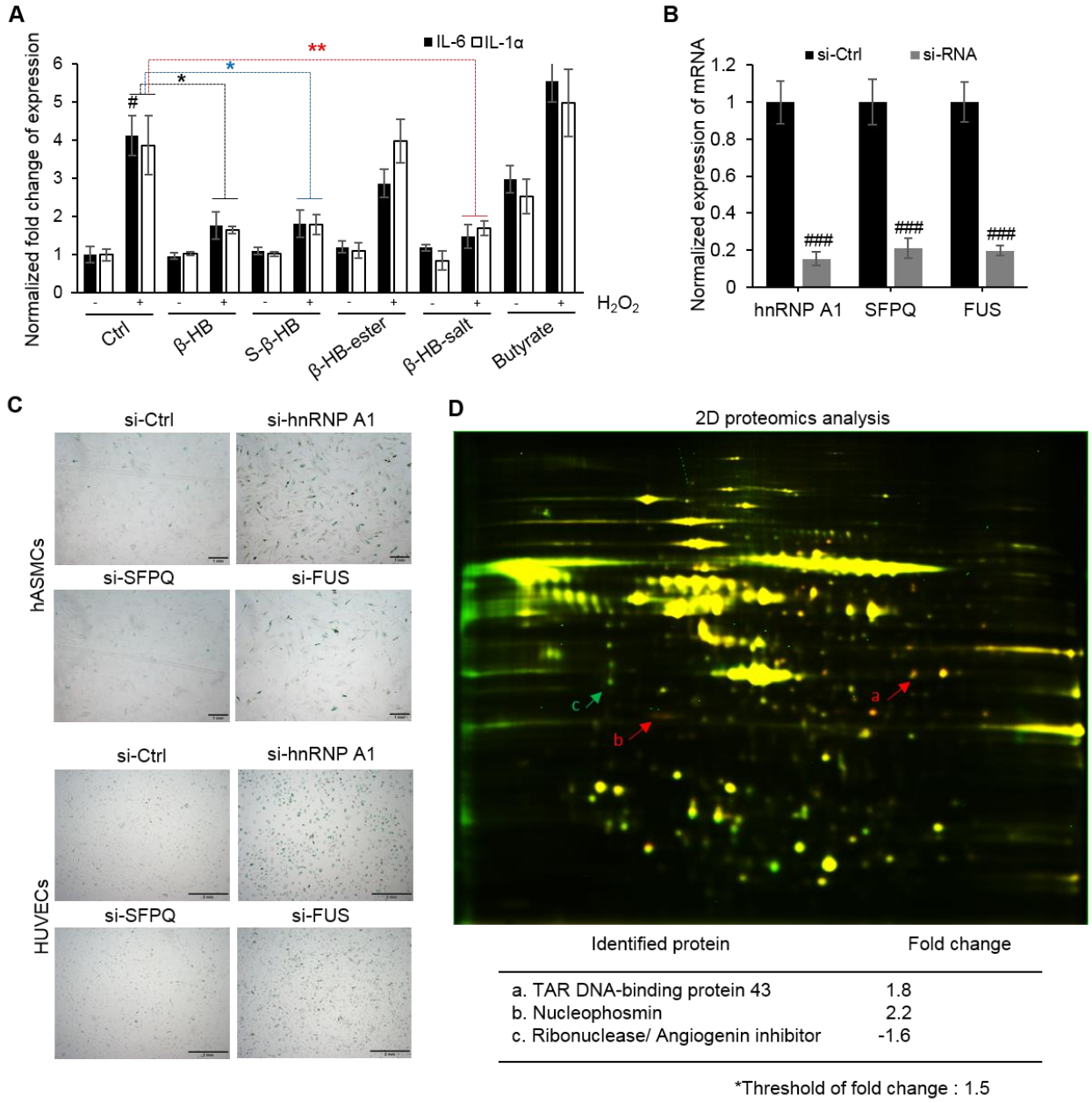

Identified protein	Fold change
a. TAR DNA-binding protein 43	1.8
b. Nucleophosmin	2.2
c. Ribonuclease/ Angiogenin inhibitor	-1.6

*Threshold of fold change : 1.5

Supplemental Figure 3 (related to Figure 3). Proteomics approach identifying the target protein of β-HB.

(A) Quantitative real-time PCR (qRT-PCR) analysis of IL-6 and IL-1α. β-HB or β-HB analogues (S-β-HB, β-HB-ester, β-HB-salt and Butyrate) was added to HUVECs culture with or without H_2O_2 (150 μM, 24 h) stimulation. n = 3, $^{\#}p < 0.05$ vehicle *vs.* H_2O_2, $^{*}p < 0.05$, $^{**}p < 0.01$ control (Ctrl) + H_2O_2 *vs.* treated group + H_2O_2.

(B) qRT-PCR analysis of hnRNP A1, SFPQ and FUS after silencing each genes to validate silencing efficiency respectively. n = 3, $^{\#\#\#}p < 0.01$ si-Ctrl *vs.* si-RNA.

(C) Representative images of SA β-gal activity assay in hASMCs or HUVECs after silencing hnRNP A1, SFPQ, or FUS. n = 3.

(D) Comparative 2D-DIGE (Difference gel electrophoresis) analysis of HUVECs treated with β-HB (4 mM) for 2 days. Control lysate was labeled with Cy3 (green) dye and β-HB treated lysate with Cy5 (red) dye. Spots were picked and analyzed using MALDI-TOF mass analysis.

Data are presented as mean ± standard error of mean (SEM).

Figure S4 (related to Figure 4).

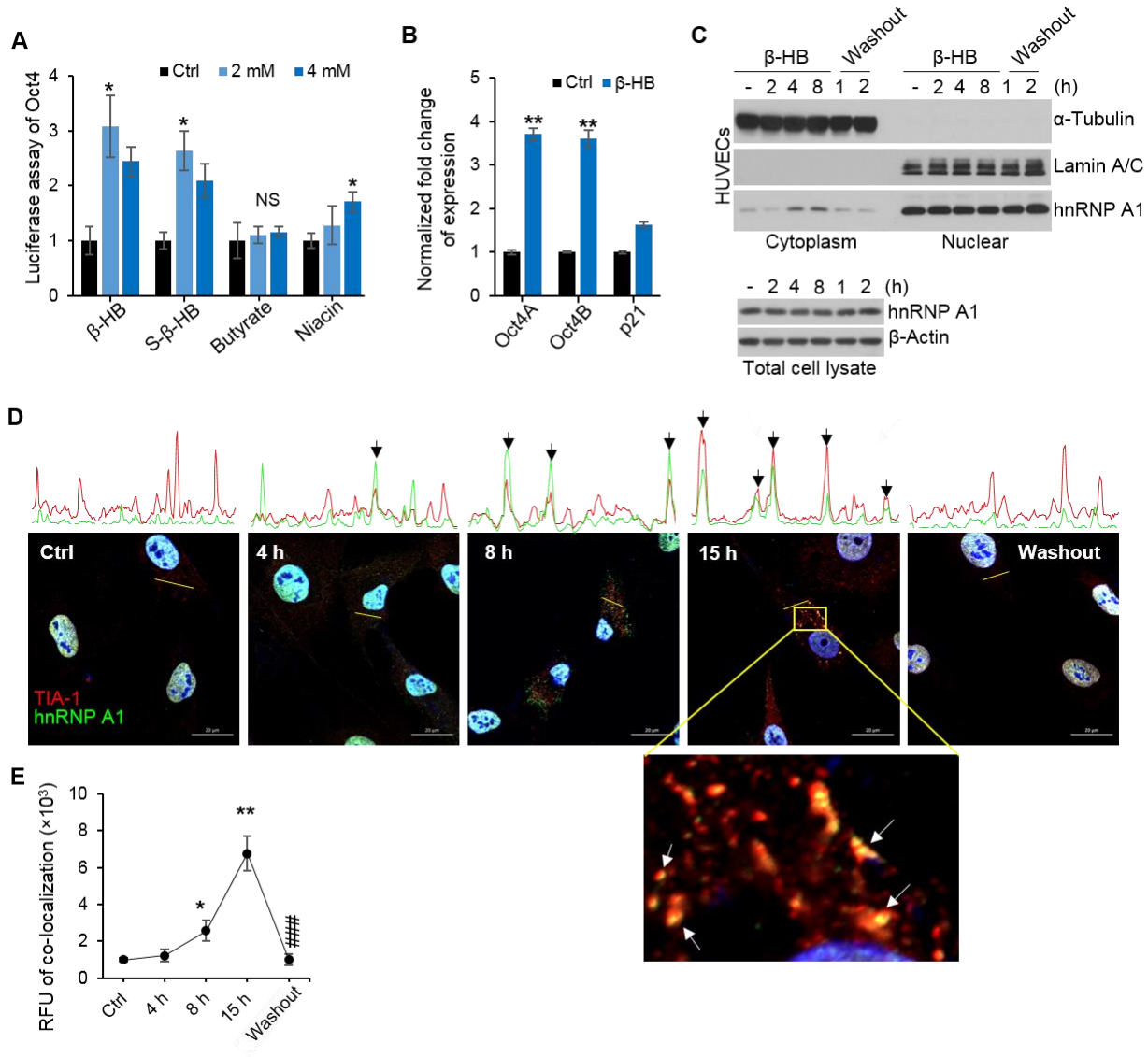

Supplemental Figure 4 (related to Figure 4). hnRNP A1-mediated stabilization of Oct4 mRNA in response to β-HB.

(A) Luciferase assay for Oct4 transcriptional activity in HUVECs treated with β-HB, S-β-HB, Butyrate, or Niacin, which have structural similarity with β-HB. n = 3. $^{*}p < 0.05$ control *vs.* treated group. NS, non-significant.

(B) qRT-PCR analysis of Oct4A, Oct4B, and p21 in HUVECs treated with β-HB (4 mM, 15 h). n = 3, $^{**}p < 0.01$ control (Ctrl) *vs.* β-HB.

(C) Representative Western blots for subcellular localization of hnRNP A1. Upper panel represents localization of hnRNP A1 in cytoplasm and nuclear fraction of HUVECs with β-HB treatment (4 mM). Lower panel represents total level of hnRNP A1 after β-HB treatment for indicated time periods. n = 3.

(D) Representative images of immunofluorescence staining of hnRNP A1 (green) and TIA-1 (red) after β-HB treatment (4 mM) at indicated time points. Linear trajectories (yellow line) crossing the cell with the two signals were presented on the top of images. Arrows indicate colocalization of TIA-1 and hnRNP A1. n = 3, Scale bar, 20 μm.

(E) Quantification of TIA-1 and hnRNP A1 colocalization in Figure S4D. $^{*}p < 0.05$, $^{**}p < 0.01$ control *vs.* β-HB treatment. $^{\#\#\#}p < 0.01$ 15 h *vs.* Washout.

Data are presented as mean ± standard error of mean (SEM).

Figure S5 (related to Figure 5).

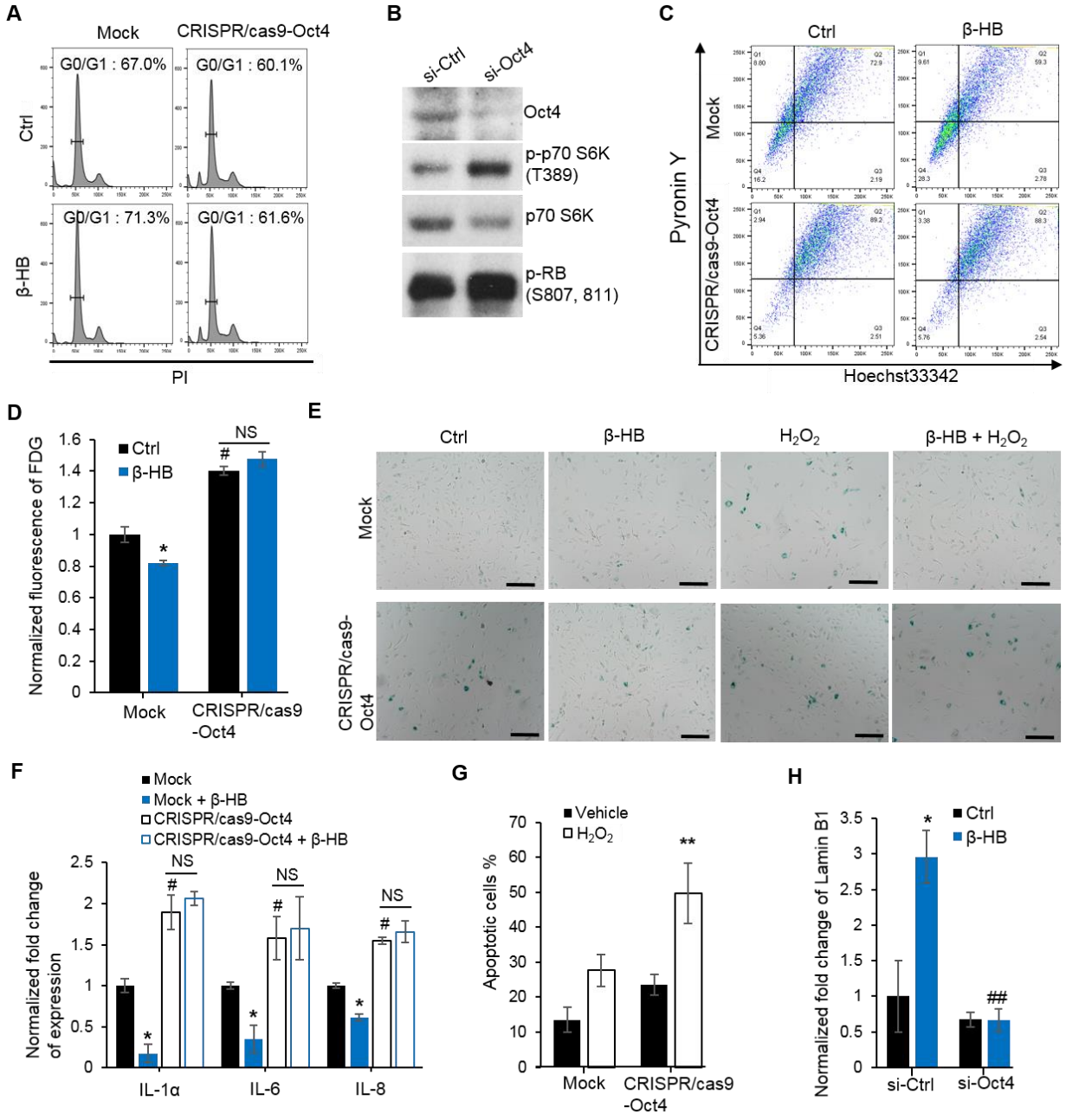

Supplemental Figure 5 (related to Figure 5). Oct4 knockdown and ectopic expression in HUVECs.

(A) Cell cycle distribution analysis of HUVECs, transfected with or without CRISPR/cas9-Oct4 plasmid to knockdown Oct4 gene expression. After transfection, β-HB (4 mM, 15 h) was treated to Mock and Oct4 knockdown group, then cells were assessed by flow cytometry analysis with PI staining. n = 3.

(B) Western blot analysis of Oct4, p-p70 S6K and p-RB in HUVECs after silencing Oct4 by siRNA.

(C) Cell cycle distribution of quiescent HUVECs (G0 phage) transfected with or without CRISPR/cas9-Oct4. After 2 days of transfection, β-HB (4 mM, 15 h) was added, then quiescent cells were assessed using flow cytometry based on 10,000 cells by staining of Pyronin Y and Hoechst 33342. n = 3.

(D) Fluorescein Di-β-D-galactopyranoside (FDG) assay for quantification of senescence-associated β-galatosidase activity in Mock and Oct4 knockdown HUVECs, transfected with CRISPR/cas9-Oct4. Excitation /emission = 490 /514 (nm). n = 3. $^{*}p < 0.05$ control (Ctrl) *vs.* β-HB, $^{\#}p < 0.05$ Mock *vs.* CRISPR/cas9-Oct4.

(E) Representative images of SA β-gal assay in Mock and Oct4 knockdown HUVECs (CRISPR/cas9-Oct4), stimulated by H_2O_2 (150 μM, 15 h) with or without β-HB treatment (4 mM, 15 h), Scale bar, 100 μm.

(F) q-RT PCR analysis of SASP (IL-1α, IL-6 and IL-8) in Mock and Oct4 knockdown group of HUVECs, transfected with CRISPR/cas9-Oct4, and the comparison of β-HB treatment (4 mM, 15 h). $^{*}p < 0.05$ vehicle vs. β-HB, $^{\#}p < 0.05$ Mock *vs.* CRISPR/cas9-Oct4, NS, non-significant.

(G) Quantitative analysis of Figure 5F. $^{**}p < 0.01$ vehicle *vs.* H_2O_2. n = 3.

(H) qRT-PCR analysis of Lamin B1 in HUVECs. After silencing Oct4 by siRNA, β-HB (4 mM, 15 h) was added to control siRNA-treated or Oct4-silenced cells. n = 3, $^{*}p < 0.05$ control (Ctrl) *vs.* β-HB, $^{\#\#}p < 0.01$ si-Ctrl + β-HB *vs.* si-Oct4 + β-HB.

Data are presented as mean ± standard error of mean (SEM). NS, non-significant; Ctrl, control; si-Ctrl, control si-RNA.

Figure S6 (related to Figure 6).

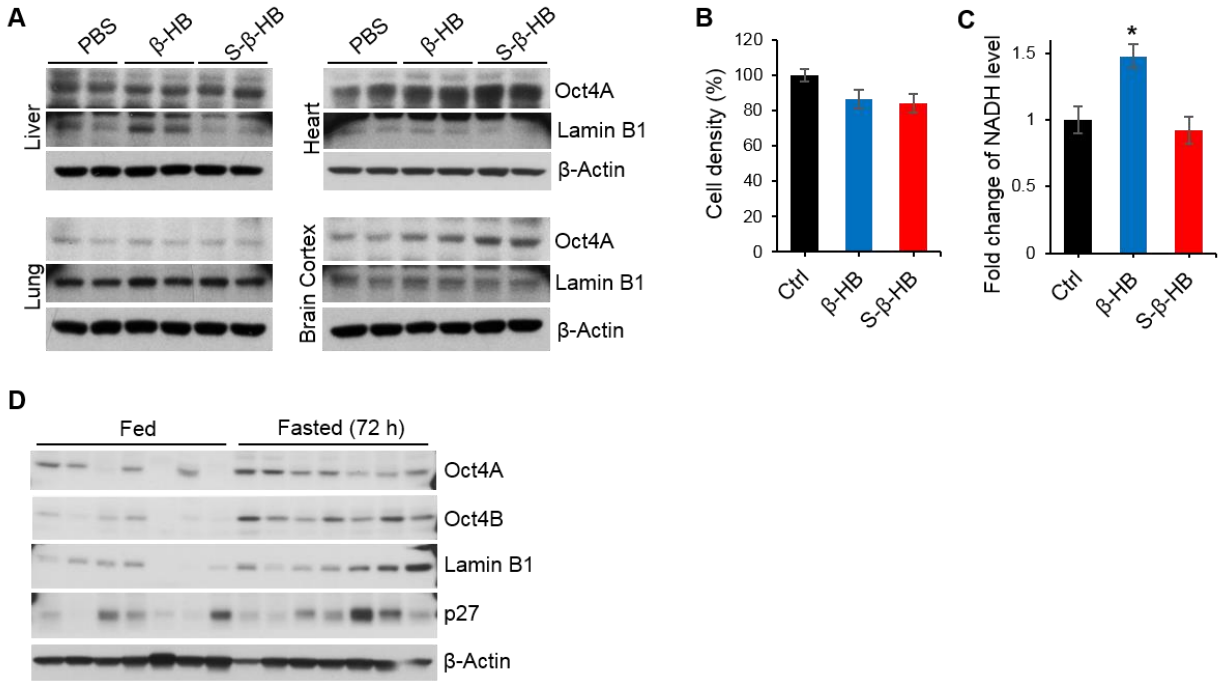

Supplemental Figure 6 (related to Figure 6). Oct4A upregulation in vascular tissues by β-HB injection or fasting.

(A) Western blot analysis of Oct4A and Lamin B1 in C57BL/6J mice organs (Liver, Lung, Heart and Brain Cortex) after intraperitonial injection with PBS, β-HB salt (1.5 g/kg) and S-β-HB (1.5 g/kg) dissolved in PBS. n = 6 mice/group.

(B) Cell density analysis of HUVECs treated with β-HB (4 mM, 24 h) or S-β-HB (4 mM, 24 h). Cells were stained with cristal violet solution to measure the cell density on the plate. n = 3, non-significant.

(C) WST-8 assay to measure NADH level produced by mitochondria in HUVECs treated with β-HB (4 mM, 24 h) and S-β-HB (4 mM, 24 h). n = 3, $^{*}p < 0.05$ control (Ctrl) *vs.* β-HB.

(D) Western blot analysis of Oct4A, Oct4B, Lamin B1 and p27 in fed or fasted mice (72 h). n = 7 mice/group.

Data are presented as mean ± standard error of mean (SEM).

Figure S7 (related to Figure 7).

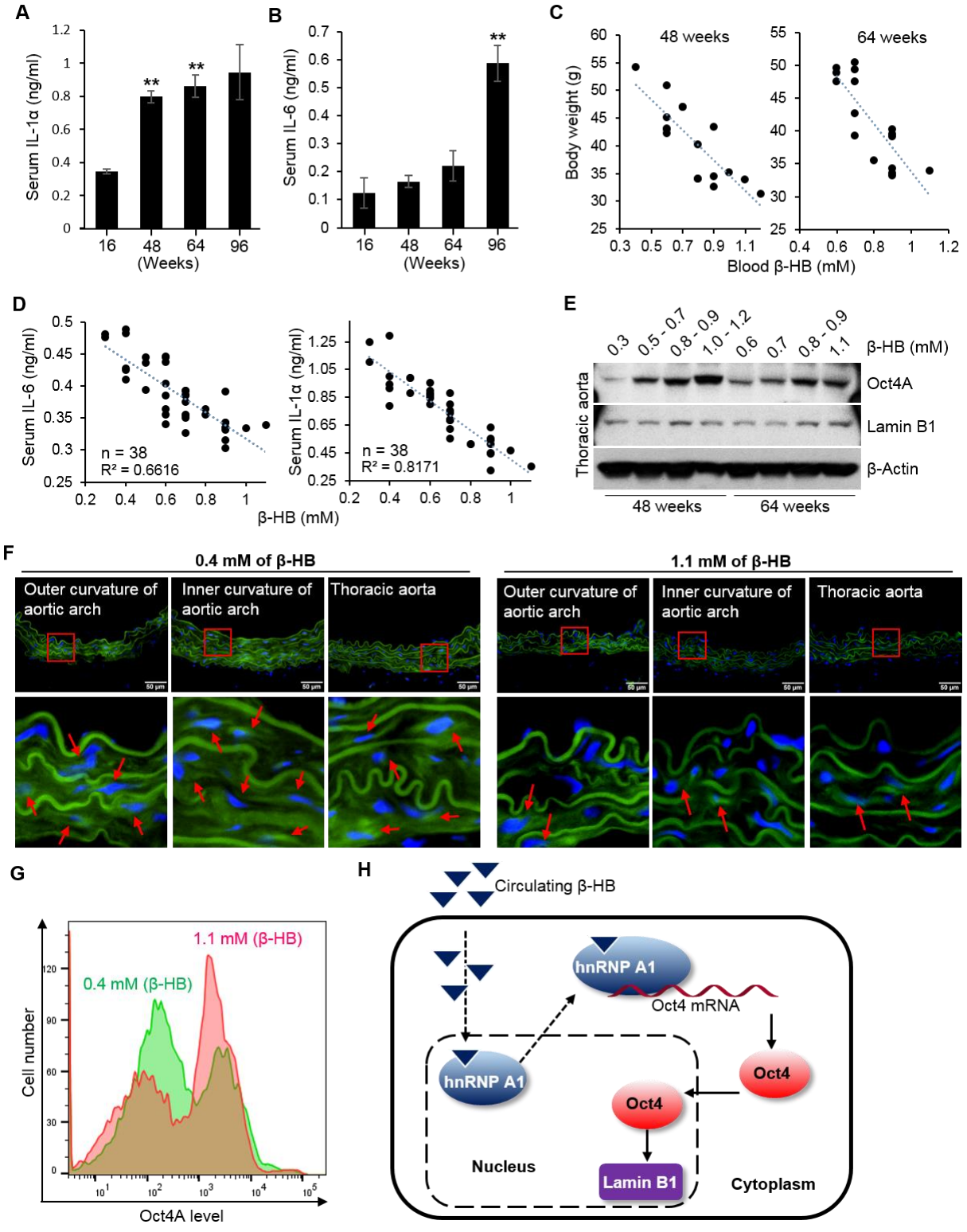

Supplemental Figure 7 (related to Figure 7). Negative correlation of senescence and circulating β-HB.

(A) Enzyme-linked immunosorbent assay (ELISA) to measure IL-1α in the different aged-mice. (n = 6-10 mice per group), $^{**}p < 0.01$ 16 weeks-old *vs.* 48 weeks- and 64 weeks-old.

(B) ELISA assay to measure IL-6 in the different aged-mice. (n = 6-10 mice per group), $^{**}p < 0.01$ 16 weeks-old *vs.* 96 weeks-old.

(C) Negative correlation of body weight and blood β-HB concentration in 48-week-old (n = 14, $R^2 = 0.6794$) and 64-week-old (n = 16, $R^2 = 0.6779$) mice.

(D) ELISA showed negative correlations of β-HB with IL-6 ($R^2 = 0.6616$) and IL-1α ($R^2 = 0.8171$) in aged C57BL/6J mice (80 weeks old, n = 38).

(E) Western blotting analyses of Oct4A and Lamin B1 in thoracic aorta from middle-aged C57BL/6J mice (48 and 64 weeks old, n =12 mice/group) stratified by blood β-HB level.

(F) Fluorogenic β-gal activity assays of aged mice aorta (inner and outer curvatures of arch and thoracic aorta). Mice were grouped according to blood β-HB level (0.4 and 1.1 mM), then SPiDer β-gal assays was performed to evaluate the site-specific effect of blood β-HB. Red arrow indicates SA β-gal positive cells. n = 5 mice/group

(G) Flow cytometry analysis of mouse primary aortic smooth muscle cells. Aortic smooth muscle cells were isolated from mice stratified by blood β-HB concentration (1.1 mM and 0.4 mM), then fixed and stained with Oct4 antibody.

(H) Schematic summary showing hnRNP A1/β-HB-mediated Oct4 upregulation.

Data are presented as mean ± standard error of mean (SEM).